RELATIVE PERFORMANCE OF DIFFERENT LMFBR LATTICE CONFIGURATIONS UNDER NATURAL CIRCULATION

by

John William Newton

RELATIVE PERFORMANCE OF DIFFERENT LMFBR LATTICE CONFIGURATIONS UNDER NATURAL CIRCULATION

by

John William Newton

B.S., United States Naval Academy
(1969)

SUBMITTED IN PARTIAL FULFILLMENT OF THE
REQUIREMENTS FOR THE DEGREE OF
MASTER OF SCIENCE

at the

MASSACHUSETTS INSTITUTE OF TECHNOLOGY

AUGUST 1970

ABSTRACT

RELATIVE PERFORMANCE OF DIFFERENT LMFBR LATTICE CONFIGURATIONS UNDER NATURAL CIRCULATION

by

John William Newton

Submitted to the Department of Nuclear Engineering on August 24, 1970, in partial fulfillment of the requirements for the degree of Master of Science

Analytic comparisons of the performance of LMFBR open-hexagonal, triangular, and square lattice configurations under natural circulation flow conditions were made. Lattices having the same volumetric compositions were compared with respect to reactivity change upon sodium voiding, pressure drop, and linear power output.

A brief study of the relative advantage of the lattices from the standpoint of reactivity change upon sodium voiding of a coolant channel showed that the open-hexagonal lattice was preferable because of its larger coolant-channel radius.

As regards hydraulic and thermal aspects, it was found that core pressure drops and linear power outputs were equivalent for the three lattices under both natural circulation and forced convection, for both laminar and turbulent flow regimes.

Consideration was given to developing more accurate relations for the hydraulic characteristics of the open-hexagonal lattice by modifying the traditional hydraulic diameter concept. Finally, some limitations of the open-hexagonal lattice as compared to the triangular lattice were discussed and necessary areas for future work were identified.

Thesis Supervisor: Michael J. Driscoll
Associate Professor of Nuclear Engineering

Thesis Supervisor: Neil E. Todreas
Assistant Professor of Nuclear Engineering

ACKNOWLEDGEMENTS

The author wishes to express appreciation for the assistance of his thesis supervisors, Dr. M. J. Driscoll and Dr. N. E. Todreas. He is indebted to the National Science Foundation and to the Nuclear Engineering Department of Massachusetts Institute of Technology for a traineeship which made work toward an advanced degree possible. He also wishes to express appreciation to Dianne Bagenski for the assistance given in preparing the final draft of this thesis.

TABLE OF CONTENTS

LIST OF FIGURES

LIST OF TABLES

Chapter 1

Introduction

1.1 Background

In liquid-metal cooled fast-breeder reactors an area of particular concern is that of loss of heat removal capability and subsequent coolant boiling. The designs for most large LMFBR's of the future include the capability for the removal of generated heat by natural circulation in the event of loss of pumping power. Most of these designs were based on the use of triangular pitch fuel pin lattices.

1.2 Objectives

The objective of this thesis is to determine the relative performance of different LMFBR lattice configurations under natural circulation with respect to the power output which could be attained during normal operation and with respect to safety considerations in the event of loss of primary pumping power in a pumped circulation system. Figures 1-1 and 1-2 describe the lattice configurations under consideration.

1.3 Discussion

Advantages of natural circulation operation include:

1. At full power operation primary pumps would be eliminated, a factor which would reduce cost of hardware and eliminate the concern of a loss of pumping power.

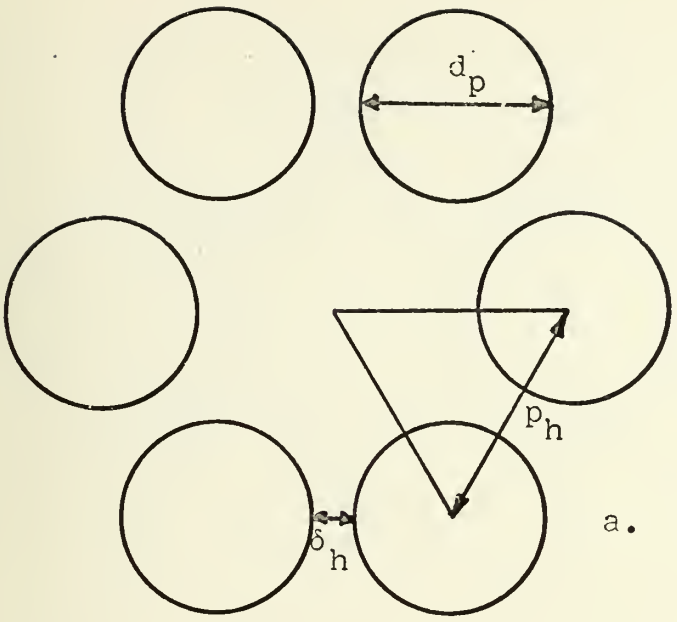

a. Open-hexagonal lattice

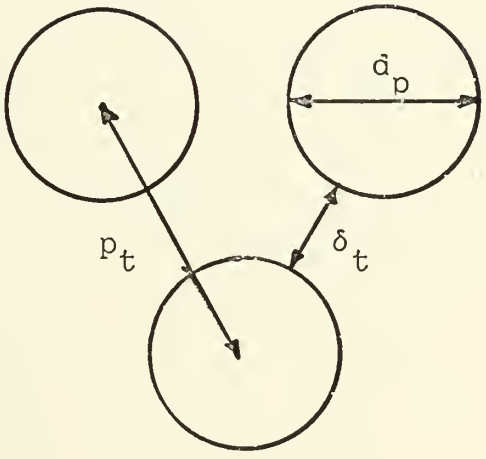

b. Triangular lattice

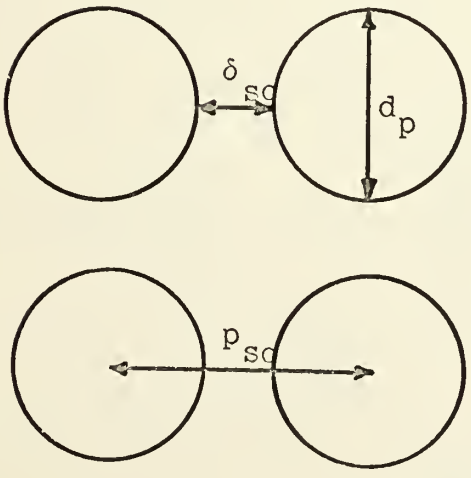

c. Square lattice

Fig. 1.1. Lattice configurations

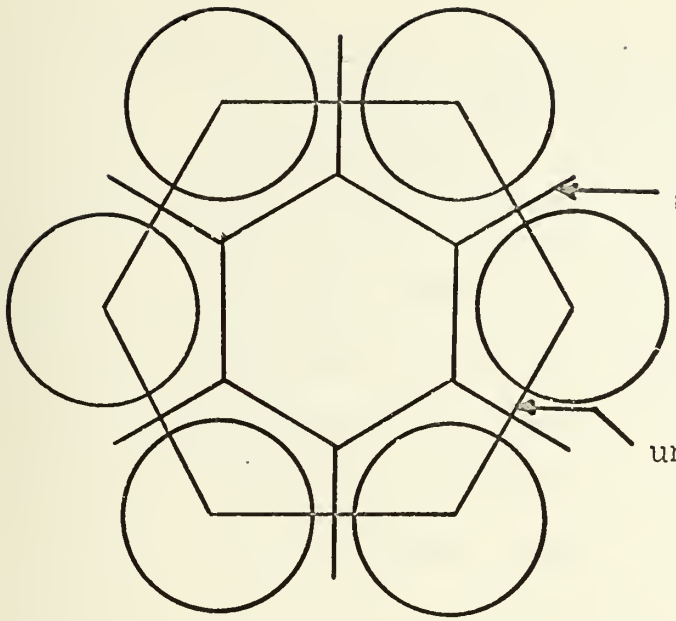

a. Open-hexagonal cell

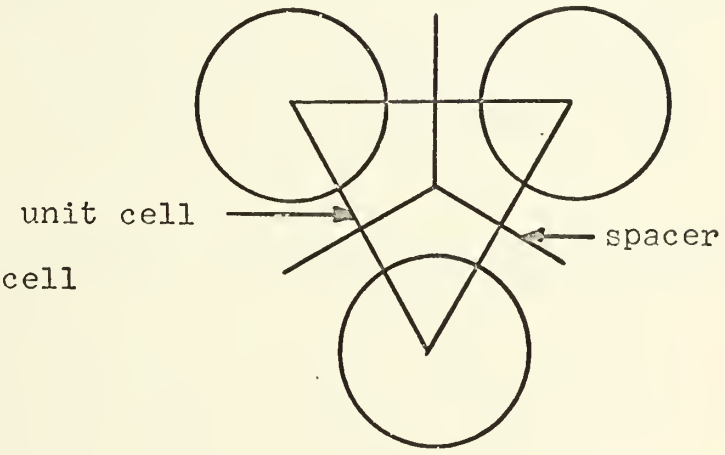

b. Triangular cell

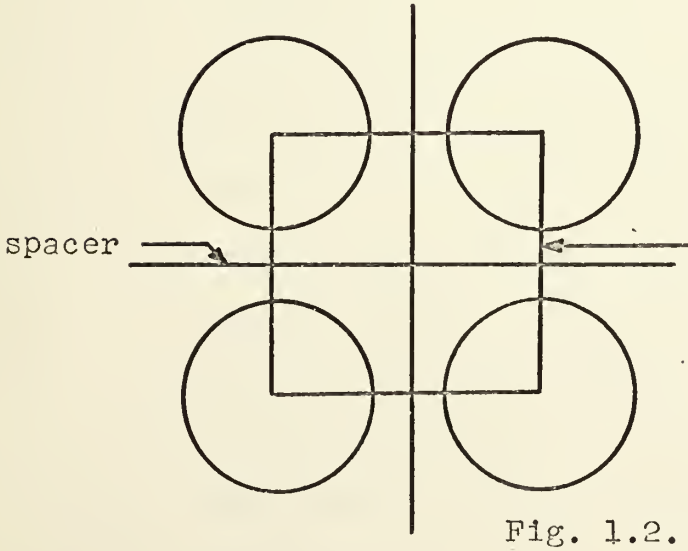

c. Square cell

Fig. 1.2. Unit cell configurations

2. At full power operation a natural circulation system would, to some extent, be self-regulating; for a given channel, as power increases/decreases, the core inlet and outlet temperature difference and the coolant mass flow rate would increase/decrease. The parallel channel problem requires further investigation, however.

3. In a pumped system natural circulation would serve as a safety measure in that the loss of primary pumping power would not result in coolant boiling and burnout since a sufficiently large natural flow could carry away the heat quickly enough.

Disadvantages of natural circulation operation include:

1. The plant will have to operate at a lower power output than would a plant with primary coolant pumps if design variables cannot adequately be optimized within various constraints.

2. The design of the system would necessitate placing the intermediate heat exchanger far above the core in order to achieve the necessary height between the core and the heat exchanger for a desired thermal driving potential. In this position the intermediate heat exchanger could complicate access to the core from above and would necessitate a larger (taller) outer containment structure.

1.4 Choice of Design Constraints and Variables

The loop-type system was chosen as the primary coolant system. Since the reactor system needs a high thermal driving head in order to attain the desired coolant flow rate, the intermediate heat exchanger needs to be above the core at a height which cannot practically be designed into a pot-type system. However, the pot-type system, through the thermal inertia of its large pool of sodium, provides ample margin for core cooling following loss of pumping power.

Sodium is by far the coolant of choice for recent LMFBR designs. Thus, in this study liquid sodium was chosen as the coolant.

The type of spacer system chosen for the open-hexagonal lattice was the grid system. Wire-wrap spacers would probably be more practical economically[1], but with the center of the open-hexagonal lattice open, each rod would have support only from three wires in one complete spiral instead of support from six wires as in a triangular pitch. The grid spacer was chosen in order that the open-hexagonal system would have the most and sufficient support against vibration.

In the comparison of the three lattices several variables will be examined. Under natural circulation the linear power output depends on a combination of core temperature rise, fuel pin diameter and pitch, fuel pin

length, and the effective heat exchanger height to primary coolant system length ratio. Combinations of the variables will be discussed with the use of typical values of current LMFBR fluid and mechanical parameters.

1.5 Synopsis

The comparison of the LMFBR lattices will first be examined from the standpoint of the additional leakage reactivity resulting from the heterogeneity of the core using the different lattices. An examination of the relative mass flow rates, core pressure drops, and linear power outputs will then be made followed by an example calculation of these quantities. In addition a more applicable expression for hydraulic diameter will be sought for an open-hexagonal lattice. Finally, conclusions and recommendations will be proposed.

Chapter 2

Reactivity Effects of Voided Coolant Channels

2.1 Reactivity Effect Components in a Sodium Voided Coolant Channel

When a coolant channel is voided of sodium, a change in reactivity occurs. This reactivity change consists of three first order components: a change in the number of neutrons captured, a shift in the neutron spectrum, and leakage of neutrons. Detailed discussion of the total sodium-void effect may be found in publications by Hummel and Okrent[2] and Monroe[3].

Most calculations of the leakage component of the change in reactivity are based on the assumption that the reactor is homogeneous. In this chapter a rough calculation of the additional leakage reactivity effect due to the heterogeneity of the core will be made. For a more detailed discussion of the leakage component of sodium-void reactivity in heterogeneous cores, the reader is refered to a study made by Lacapelle[4] whose method was based on the work of Benoist[5]. The leakage component of the overall reactivity change will be compared in the open-hexagonal and triangular lattices showing that the larger hole of the open-hexagonal cell results in a greater negative reactivity than does the hole in the triangular cell. The calculations used in the comparison are based on formulations derived in Behren's original paper "The Effect of Holes in a Reacting Material on the Passage of Neutrons"[6].

2.2 Leakage Reactivity Calculations for Open-hexagonal and Triangular Lattices

Comparing Behren's Eq. (8) and Eq. (10) for closely spaced, interacting holes in a medium having a long mean free path we have

$$\frac{L^2}{L_0^2} = 1 + 2\phi + \phi^2 + \frac{Qr_{hy}\phi}{\lambda} \quad , \tag{2-1}$$

where

ϕ is the volume ratio of the holes to the material of the reactor,

Q is a function of the shape of the hole,

λ is the mean free path in the solid,

$r_{hy} \equiv \frac{2\phi\nu}{S}$ is the nuclear hydraulic radius of the cell,

ν is the volume of the cell of material surrounding each hole,

S is the surface area of each hole,

L_0^2 is the mean square direct distance travelled by a neutron in the course of N collisions in a homogeneous medium,

L^2 is the mean square direct distance travelled by a neutron in the course of N collisions in a medium with holes,

The change in reactivity is given by

$$\frac{\delta k}{k} = -\left(\frac{\delta D}{D_{Hom}}\right)(k_\infty - 1)/k_\infty \, . \tag{2-2}$$

The definition of diffusion length gives

$$\frac{L^2}{L_0^2} = \frac{D\Sigma_a^0}{D_0\Sigma_a} = (1 + \phi)\frac{D}{D_0} \, , \tag{2-3}$$

since

$$\Sigma_a = \frac{\Sigma_a^0 V_{fuel}}{V_{tot}} = \frac{\Sigma_a^0 V_{fuel}}{(V_{fuel} + V_{hole})} = \frac{\Sigma_a^0}{(1 + \phi)} \quad . \qquad (2\text{-}4)$$

Equating Eqs. (2-1) and (2-3)

$$(1 + \phi)\frac{D}{D_0} = (1 + \phi)^2 + \frac{Qr_{hy}\phi}{\lambda}$$

or

$$D = D_0(1 + \phi) + \frac{Qr_{hy}\phi}{3(1 + \phi)} \quad . \qquad (2\text{-}5)$$

The change in the diffusion coefficient is

$$\delta D = D - D_{Hom} = \frac{Qr_{hy}\nu_{hole}}{3} \qquad (2\text{-}6)$$

where

D_{Hom} is the homogeneous value of the diffusion coefficient

$\nu_{hole} = \frac{\phi}{1 + \phi}$ is the volume fraction of holes

For a first approximation we will assume that the cells in our theoretical core are cylindrical. The volume of each cylindrical hole will be set equal to the actual volume of coolant channel associated with a cell, and the volume of fuel material surrounding each hole will be set equal to the actual volume of fuel material associated with a cell. Refer to Fig. 1.2 for the unit cell configurations chosen. Note

that the cells are based on the coolant channel and not on a fuel rod as is the more common convention. When this approximation is made, the nuclear hydraulic radius, r_{hy}, is the same as the actual radius of the equivalent cylindrical coolant cell.

Refer to Fig. 1.1.a for a definition of parameters needed to find the hydraulic radius of the open-hexagonal cell:

$$A_{hole} = A_{tot} - A_{fuel} ,$$

$$\pi(r_{hy})_h^2 = \frac{6\sqrt{3}}{4} p_h^2 - \frac{4\pi}{8} d_p^2 ,$$

$$(r_{hy})_h = \frac{1}{2}\left(\frac{6\sqrt{3}}{\pi} p_h^2 - \frac{4}{2} d_p^2\right)^{1/2} . \qquad (2\text{-}7)$$

Refer to Fig. 1.1.b for the hydraulic radius of the triangular lattice:

$$A_{hole} = A_{tot} - A_{fuel} ,$$

$$\pi(r_{hy})_t^2 = \frac{\sqrt{3}}{4} p_t^2 - \frac{\pi}{8} d_p^2 ,$$

$$(r_{hy})_t = \frac{1}{2}\left(\frac{\sqrt{3}}{\pi} p_t^2 - \frac{1}{2} d_p^2\right)^{1/2} . \qquad (2\text{-}8)$$

Since $p_h = (2/3)^{1/2} p_t$, then

$$(r_{hy})_h = \frac{2}{2}\left(\frac{\sqrt{3}}{\pi} p_t^2 - \frac{1}{2} d_p^2\right)^{1/2} = 2(r_{hy})_t . \qquad (2\text{-}9)$$

Inserting Eq. (2-6) into Eq. (2.2):

$$\frac{\delta k}{k} = -\left(\frac{Q r_{hy} \nu_{hole}}{3 D_{Hom}}\right)\left(\frac{k_\infty - 1}{k_\infty}\right) . \qquad (2\text{-}10)$$

Using the following typical values for an open-hexagonal and a triangular lattice:

$Q = 4/3$ (as tabulated in ref. (6)),

$\nu_{hole} = 1 - \nu_{fuel} = 0.528$,

$p_t = 0.416$ in.,

$p_h = 0.340$ in.,

$d_p = 0.300$ in.,

$D_{Hom} = 4$ cm $= 1.57$ in. for a voided core,

$k_\infty = 1.5$,

the ratio of reactivity changes is

$$\frac{(\delta k/k)_h}{(\delta k/k)_t} = 2 .$$

Solving for the reactivity changes:

$$(\delta k/k)_t = -0.0056 = -\$1.70$$

$$(\delta k/k)_h = -0.0112 = -\$3.40$$

using $\beta = 0.0033 \equiv \$1.00$.

For a square lattice with

$\nu_{hole} = 0.528$

$d_p = 0.300$ in.

$p_s = 0.388$ in.

$$\frac{(\delta k/k)_h}{(\delta k/k)_{sq}} = 1.42$$

and

$$(\delta k/k)_{sq} = -\$2.40 \quad .$$

From the above calculations we can see that the open-hexagonal lattice results in a higher negative reactivity from leakage in a voided coolant channel than do triangular or square lattices of the same volume fraction of fuel. Because of its higher negative reactivity the open-hexagonal lattice is preferable to both the triangular and the square lattices from the standpoint of keeping the effective increase in multiplication factor as low as possible upon sodium voiding of coolant channels.

In the next chapter the relative mass flow rates, core pressure drops, and linear power outputs of the three lattices will be compared. These comparisons will be used in determining which lattice is preferable from hydraulic and power removal aspects.

Chapter 3

Expressions for and Comparison of Mass Flow Rates, Pressure Drops and Linear Power Output for Different LMFBR Lattice Configurations

3.1 Discussion

As was seen in Chapter 2, the hexagonal lattice proved to be more advantageous than a triangular or square lattice from a leakage reactivity standpoint. In this chapter the three lattices will be compared with respect to some hydraulic and power aspects to see if the larger hole of the open-hexagonal lattice renders it preferable to both the square and triangular lattices. In the present chapter the three lattices will be compared on an equivalent basis, namely, equal rod size and fuel volume fraction, with respect to pressure drops and linear power output. It will be assumed that all fluid properties are equal for the three lattices.

As will be seen in the numerical examples of Chapter 4, the core pressure drops of the three lattice arrangements are essentially the same for equal fuel volume fraction and equal coolant velocities. The only differences in pressure drop are due to the differences in spacer arrangement of the different lattices, and these differences are small. Therefore, these small pressure drop differences can be neglected in a first order approximation of the relative linear power output for the three lattice arrangements. However, in the

calculation of the absolute linear power output for any given lattice, the spacer pressure drop contribution to the total core pressure drop cannot be neglected since it constitutes as much as 45% of the total core pressure drop.

3.2 Procedure for Calculation of Core and Spacer Pressure Drop

The total pressure loss, ΔP_T, through the reactor core, hence, through a unit cell flow path in the core, consists of three factors: pressure loss at bundle entrance and exit, ΔP_E; frictional pressure loss without spacers, ΔP_R; pressure loss due to spacers, ΔP_S. It will be assumed that pressure loss at the bundle entrance and exit will be equal for all three lattices. This assumption is based on the fact that the entrance and exit openings are of equal total cross sectional area for the cores containing the different lattices and that the coolant velocities in the three cores are equal. By using equations similar to Eqs. (3-1) and (3-2), one can find that the entrance and exit losses for the different cores are the same.

Since there is no experimental data on pressure drops through open-hexagonal rod bundles with and without spacer devices known to the author, the approach for calculating the semi-empirical pressure drop through an open-hexagonal lattice will be as follows. Tong's [7] method for finding the theoretical pressure drop through a channel with spacers is used to find theoretical values of ΔP_S for the triangular

and open-hexagonal lattices. Then a ΔP_S is found from experimental data gathered and correlated by de Stordeur[8] for triangular lattices. A ratio of experimental to theoretical spacer pressure drops is then obtained for triangular lattices. The theoretical pressure drop for the open-hexagonal lattice calculated from Tong's formulae are then multiplied by the ratio found above to obtain an appropriate semi-empirical spacer pressure loss for the open-hexagonal lattice. This approach thus uses the existing experimental data of de Stordeur to normalize the calculated results from Tong's method which is applicable, unlike de Stordeur's data, to both triangular and open-hexagonal lattices.

3.3 Theoretical Core and Spacer Pressure Drop

According to Tong "the pressure losses in a rod bundle due to the rod spacers are the form drag type pressure loss. This type of pressure drop can be calculated by using the pressure loss coefficients at sudden contraction, K_c, and at sudden expansion, K_e, as given by Kays and London[11]". (7) Values of K_c and K_e are reproduced in Fig. 3.1. The pressure losses at sudden contractions and expansions are given as follows:

For a sudden contraction

$$\Delta P_c = \frac{\rho V_2^2}{2g_c}(1-\sigma^2) + K_c\frac{\rho V_2^2}{2g_c} \quad \text{per spacer.} \qquad (3\text{-}1)$$

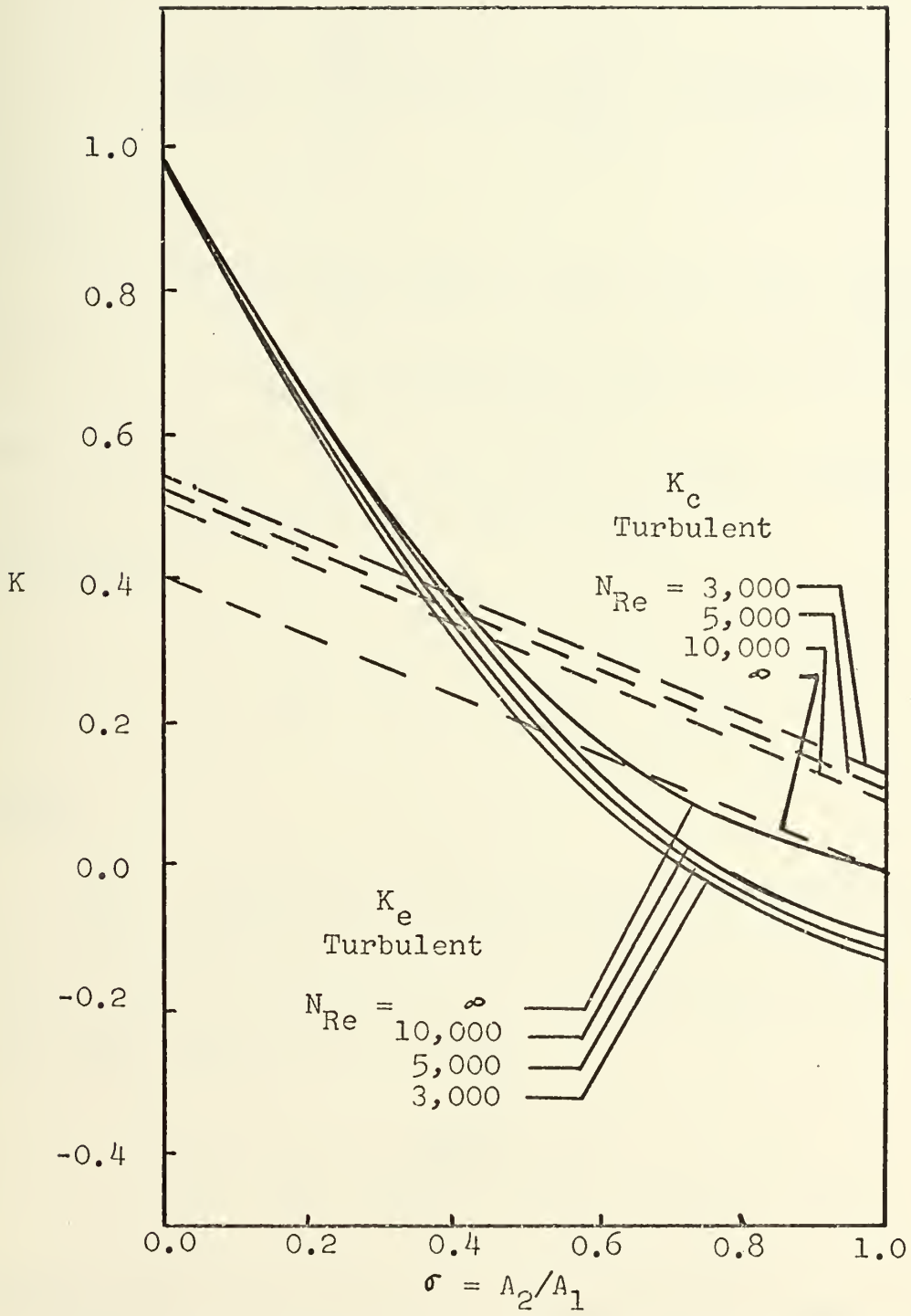

Fig. 3.1. Pressure loss coefficients at sudden contraction , K_c, and at sudden expansion, K_e, as given by Kays and London[9]. Taken from Ref. (7), Fig. 7.

For a sudden expansion

$$\Delta P_e = - \frac{\rho V_2^2}{2g_c}(1-\sigma^2) - K_e \frac{\rho V_2^2}{2g_c} \quad \text{per spacer,} \qquad (3\text{-}2)$$

where

$\sigma = A_2/A_1$ is the ratio of the flow in the gridded region to the flow area away from the gridded region,

V_2 is the velocity in the restricted cross-section region of the channel.

Note that positive ΔP's are pressure losses. Refer to Fig. 3.2 for definition of flow areas.

Therefore,

$$\Delta P_T - \Delta P_E = \Delta P_R \frac{f}{f_{cir}} + (\Delta P_S) \quad , \qquad (3\text{-}3)$$

where

$\frac{f}{f_{cir}}$ is the ratio of the friction factors in non-circular to circular channels; see Fig. 3.3[10].

Substituting an expression for the friction pressure drop in a duct into Eq. (3-3) gives

$$\Delta P_T - \Delta P_E = f_F \frac{4\rho l \bar{V}_1^2}{D_e 2g_c} \left(\frac{f}{f_{cir}}\right) + \Delta P_c + \Delta P_e \quad . \qquad (3\text{-}4)$$

Substituting expressions for ΔP_c and ΔP_e from Eqs. (3-1) and (3-2) into Eq. (3-4)

$$\Delta P_T - \Delta P_E = f_F \frac{4\rho l \bar{V}_1^2}{D_e 2g_c} \left(\frac{f}{f_{cir}}\right) + (K_c + K_e) \frac{\rho (A_1/A_2)^2 V_1^2}{2g_c} n_g \qquad (3\text{-}5)$$

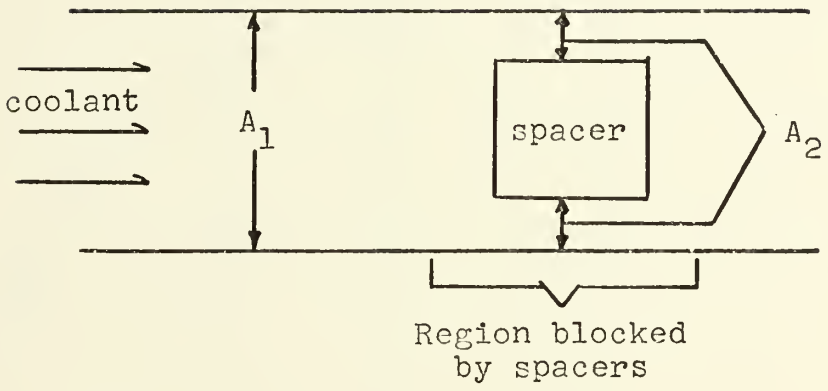

Fig. 3.2. Flow areas in a coolant cell. A_1 is the area away from the spacer region. A_2 is the free flow area in the spacer region.

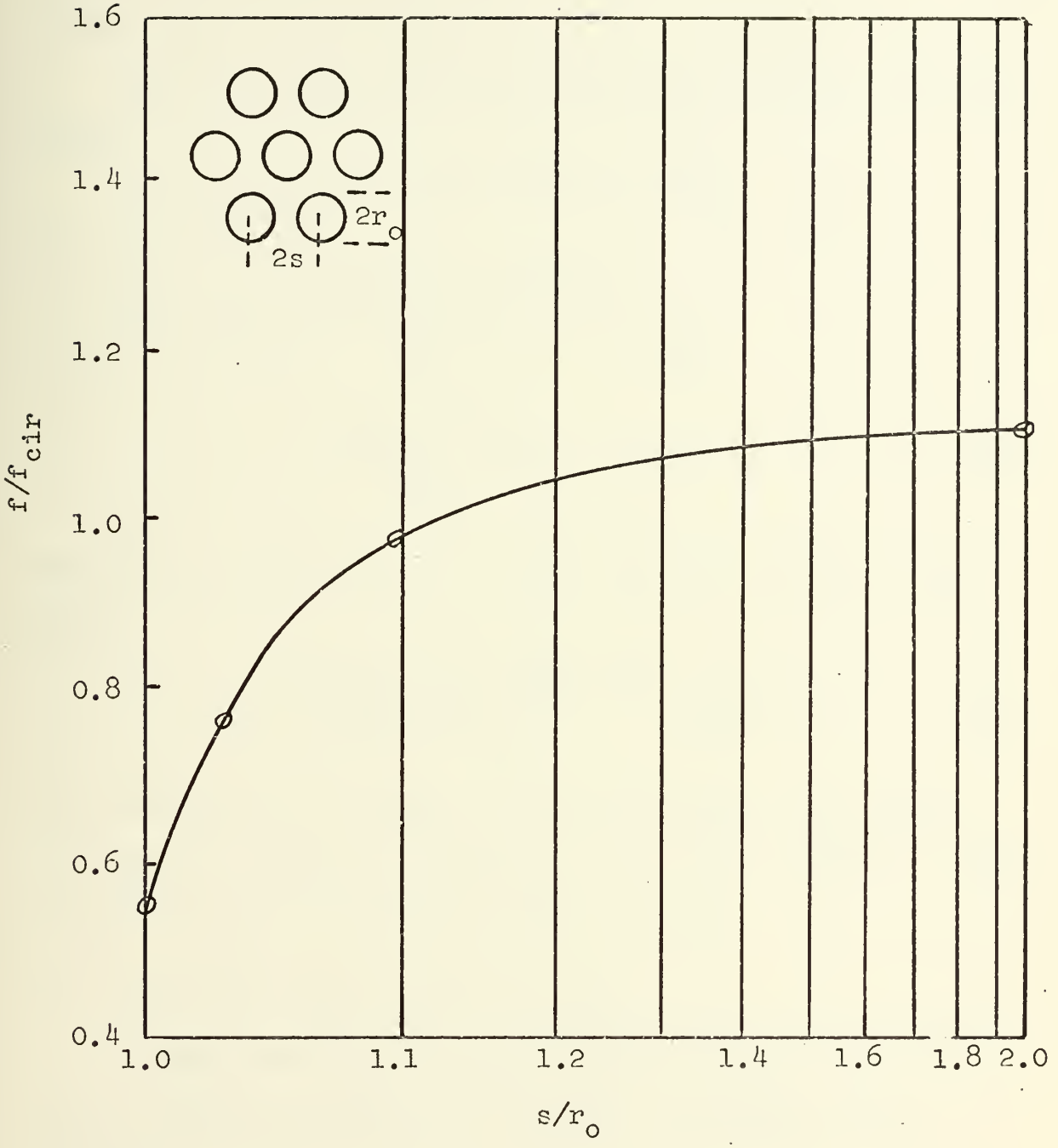

Fig. 3.3. Fully developed turbulent flow parallel to a bank of circular tubes of rods; points ⊙ based on friction coefficients calculated by Deissler and Taylor[11] at Re = 10^5; Reynolds number influence is small, and Nusselt number behavior is virtually the same as friction behavior. Taken from Ref. (10), Fig. (9-10), which also shows that the ratio of Nusselt numbers is similar to the ratio of friction factors for non-metalic fluids.

where

n_g is the number of spacer grid sets in the rod bundle.

Using

$f_F = 0.046\ Re^{-0.2}$ for turbulent flow,

Eq. (3-5) becomes

$$\Delta P_T - \Delta P_E = \frac{0.092\mu^{0.2}l\rho^{0.8}V_1^{1.8}}{D_e^{1.2}g_c}\left(\frac{f}{f_{cir}}\right) + \frac{\rho(A_1/A_2)^2V_1^2}{2g_c}(K_e + K_c)n_g \quad , \qquad (3\text{-}6)$$

where $\bar{V}_1$ is found from $\bar{V} = \bar{\omega}/\rho A_1$ (ft/hr), and $\bar{\omega}$ is found from

$$\bar{\omega} = \left(\frac{g\beta\rho^2 Z_e D^{1.2}S^{1.8}\bar{q}_T}{0.092\mu^{0.2}Nc_p}\right)^{0.357} \quad \text{(lb/hr)} \quad . \qquad (A\text{-}8)$$

The quantity $\bar{\omega}$ is the average mass flow rate for natural circulation derived in Appendix A, n_r is the number of effective rods per cell and $\bar{q} = n_r\bar{q}'l$.

3.4 Empirical Spacer Pressure Drop

An empirical ΔP_S for a triangular lattice will now be found using de Stordeur's[8] method. According to de Stordeur

$$\Delta P_S = \frac{C_S V_S^2 S\rho}{2gA_1} \qquad (3\text{-}7)$$

where

C_S is the spacer drag coefficient

V_S is the velocity in the spacer region (ft/sec)

S is the spacer projected frontal area (ft^2)

g is the gravitational acceleration (ft/sec^2)

A_1 is the flow area in the cell away from the gridded region (ft^2)

ρ is the density of the coolant (lb/ft^2)

ΔP_S is the pressure loss due to one spacer (lb/ft^2)

Using appropriate values of V_S, S, g, A_1, ρ, and a C_S taken from Fig. 3.4, an empirical spacer pressure drop, ΔP_S, can be calculated from Eq. (3-7) for a triangular lattice with a honeycomb pin support grid.

We can now obtain the ratio of the empirical spacer pressure drop to the theoretical spacer pressure drop for a triangular lattice with a honeycomb grid and set it equal to the ratio of the empirical to theoretical spacer pressure drop for an open-hexagonal lattice:

$$\left[\frac{(\Delta P_S)_{em}}{(\Delta P_S)_{th}}\right]_t = \left[\frac{(\Delta P_S)_{em}}{(\Delta P_S)_{th}}\right]_h \quad . \tag{3-8}$$

An appropriate $(\Delta P_S)_{em}$ can be found from Eq. (3-8) for an open-hexagonal lattice after a $(\Delta P_S)_{th}$ for the open-hexagonal lattice has been calculated using Tong's method. Equation (3-6) then becomes

$$(\Delta P_T - \Delta P_E)_h = \frac{0.092\mu^{0.2}{}_1\rho^{0.8}V_1^{1.8}}{D_e^{1.2}g_c}\left(\frac{f}{f_{cir}}\right) +$$

$$\left(\frac{(\Delta P_S)_{em}}{(\Delta P_S)_{th}}\right)_t \frac{\rho(A_1/A_2)^2V_1^2}{2g_c}(K_e + K_c)n_g \quad . \tag{3-9}$$

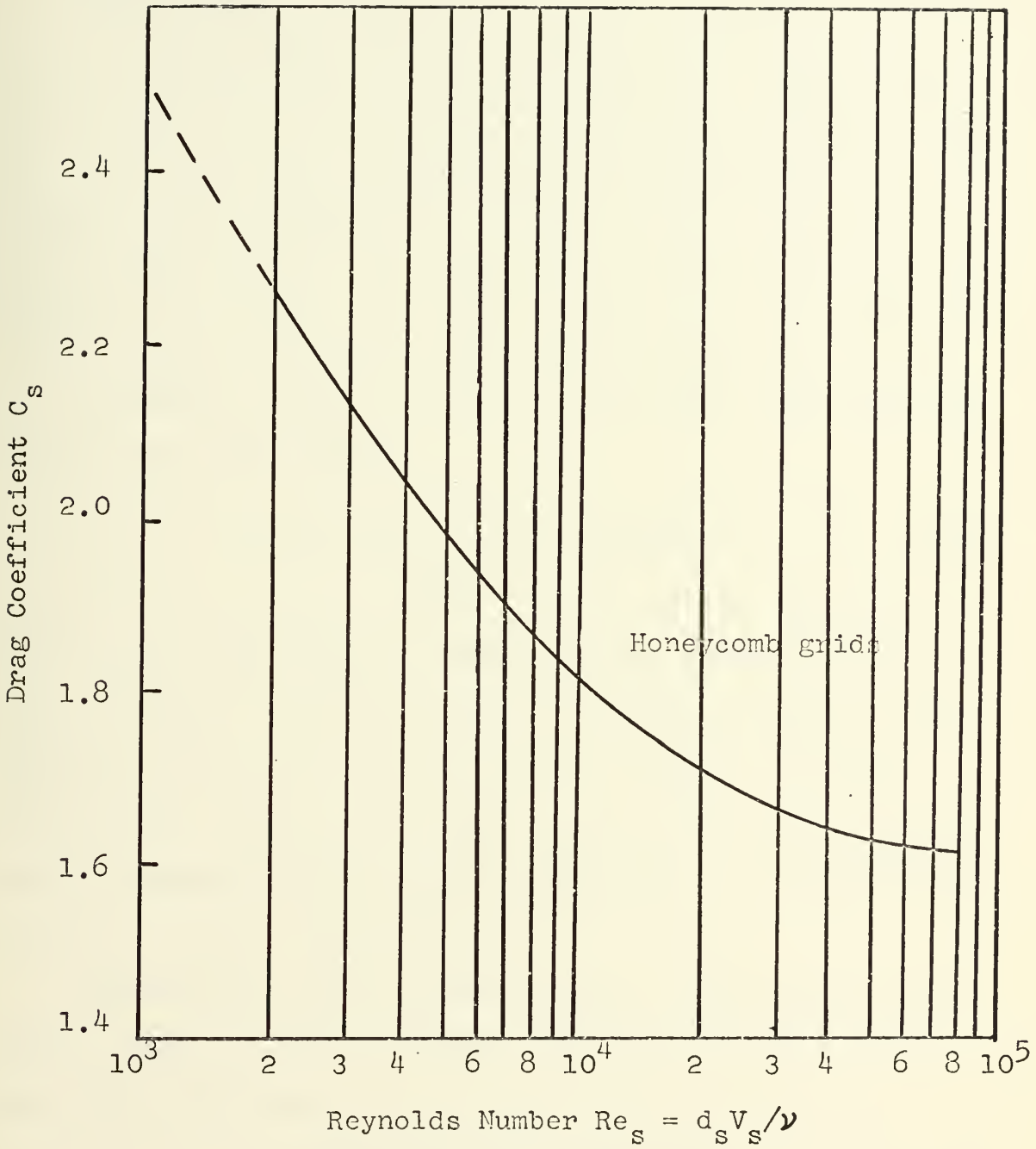

Fig. 3.4. Drag coefficients for honeycomb grid spacer. (Dashed line is an extrapolated portion of the curve.) The quantity d_s is the spacer width.[8]

3.5 Mass Flow Rate and Linear Power in Steady-State Thermal Circulation

In steady-state thermal circulation the thermal buoyancy driving force, ΔP_B, equals the friction pressure drop, ΔP_R, for a pipe loop including the rod bundle section. See Appendix A for a derivation of mass flow rate and linear power relationships. For a rod bundle section the pressure losses through the spacers adds another component to the total pressure loss in the loop. The steady state pressure balance will then become

$$\Delta P_B = \Delta P_R \frac{f}{f_{cir}} + \Delta P_S = f_s \Delta P_R \quad , \qquad (3\text{-}10)$$

where f_s is a multiplying ratio which accounts for spacer pressure drop. It is introduced in order to make the calculation of mass flow rates, pressure drops, and linear power output easier. The factor f_s is found to be approximately constant for the range of velocities investigated in any given lattice configuration.

Substituting the relationships for ΔP_B from Eq. (A-3) and ΔP_R from Eq. (A-5) into Eq. (3-10) and solving for the mass flow rate gives

$$\bar{\omega} = \left(\frac{g\beta\rho^2 Z_e D^{1.2} S^{1.8} n_r \bar{q}'1}{0.092\mu^{0.2} N c_p f_s}\right)^{0.357} \quad , \qquad (3\text{-}11)$$

where $\bar{\omega}$ is the mass flow rate for a unit cell.

As shown in Eq. (A-3) the thermal buoyancy pressure gain

depends on the linear power and the mass flow rate, and the friction pressure drop depends on the mass flow rate. These dependencies can be seen in Fig. 3.5. In Fig. 3.5 Eq. (3-11) is the locus of points along the $\Delta P_R f_s$ line, and for any given $\bar{q}'_i$ the corresponding $\bar{\omega}$ can be taken from the graph. The dashed lines represent constant $t_h - t_c$ lines. Since

$$\bar{q}' = \frac{c_p \Delta t}{n_r l} \quad , \tag{3-12}$$

for any given core lattice geometry, any one of the three variables $\bar{q}'$, $\bar{\omega}$, Δt can be found, given the other two. Solutions for a natural circulation operating condition will be the point of intersection of the three lines representing ΔP_s for a given $\bar{q}'$, $\Delta P_R f_s$, and Δt. Substituting Eq. (3-11) into Eq. (3-12)

$$\bar{q}' = \left(\frac{g\beta\rho^2 Z_e D_e^{1.2} S^{1.8} n_r}{0.092\mu^{0.2} N f_s}\right)^{0.555} \left(\frac{\Delta t}{n_r}\right)^{1.555} \left(\frac{c_p}{l}\right)^{1.0} \tag{3-13}$$

Equation (3-13) is the relationship for the intersection of the $\Delta P_R f_s$ line in Fig. 3.6 with a given Δt. The quantities $\bar{\omega}$ and ΔP_B are taken into account in Eq. (3-13).

3.6 Comparison of Linear Power Output in Open-hexagonal, Triangular, and Square Lattices

As shown in Fig. 1.2, the number of effective rods per cell for the three lattices is

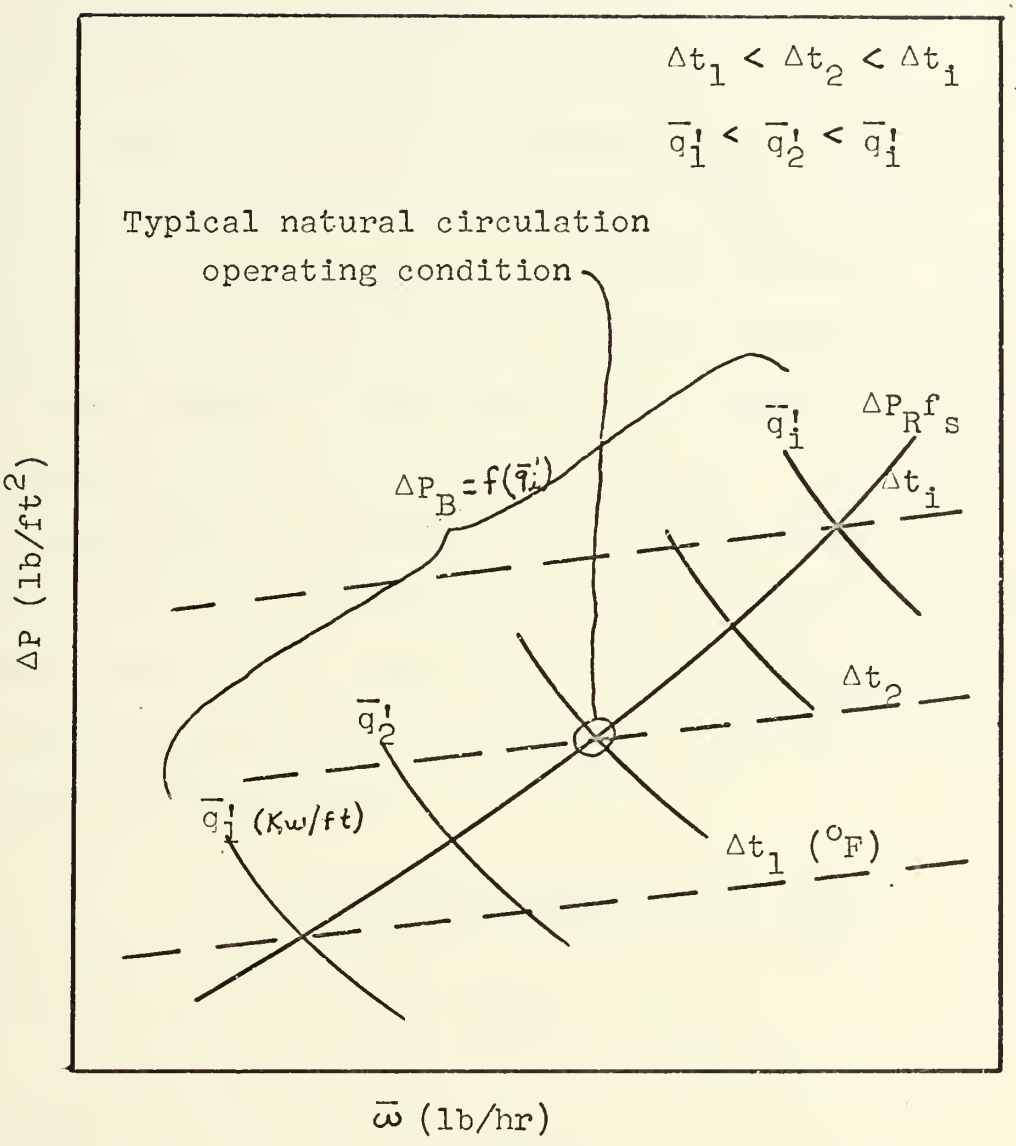

Fig. 3.5. Illustrative graph of solutions for natural circulation operating conditions. The intersection of the three lines defines an operating condition. The $\Delta P_R f_s$ line is defined by Eq. (A-6). ΔP_B lines are defined by Eq. (A-3). The Δt lines are governed by Eq. (A-11).

open-hexagonal - $n_r = 2$

triangular - $n_r = 1/2$

square - $n_r = 1$

For this comparison it will be assumed for a first order approximation that the fluid properties of the coolant, Δt, Z_e, f_s, and N_e are equal for the three lattices. The three lattices will be compared by taking a ratio of the linear power outputs of the three lattices based on equal fuel volume fraction and equal pin diameters. The variables will be the equivalent diameter, D_e, of a flow cell, the cross-sectional flow area, S, of a cell, and the number of effective fuel rods per cell, n_r. As shown in Appendix B, for equal V_f' the hydraulic diameters of the three lattices are equal. By definition

$$D_e = \frac{4 \text{ x cross sectional area}}{\text{wetted perimeter}} = \frac{4S}{P_w} ,$$

or

$$S = \frac{P_w D_e}{4} .$$

Therefore,

$$S_h = \frac{\pi d D_e}{2} ,$$

$$S_t = \frac{\pi d D_e}{8} ,$$

$$S_{sq} = \frac{\pi d D_e}{4} .$$

Using Eq. (3-13) for $\bar{q}'$,

$$\bar{q}' = \left(\frac{g\beta\rho^2 Z_e D_e^{1.2} S^{1.8} n_r}{0.092^{0.2} Nf}\right)^{0.555} \left(\frac{\Delta t}{n_r}\right)^{1.555} \left(\frac{c_p}{1}\right)^{1.0}, \quad (3\text{-}13)$$

we obtain the following ratios of linear power output:

$$\frac{\bar{q}'_h}{\bar{q}'_t} = \frac{(S^{1.8} n_r)_h^{0.555} (1/n_r)_h^{1.555}}{(S^{1.8} n_r)^{0.555} (1/n_r)_h^{1.555}}$$

$$= \frac{((\pi d D_e/2)^{1.8}(2))^{0.555} (1/2)^{1.555}}{((\pi d D_e/8)^{1.8}(1/2))^{0.555} (1/0.5)^{1.555}} \equiv 1$$

$$\frac{\bar{q}'_h}{\bar{q}'_{sq}} = \frac{((\pi d D_e/2)^{1.8}(2))^{0.555} (1/2)^{1.555}}{((\pi d D_e/4)^{1.8}(1))^{0.555} (1/1)^{1.555}} \equiv 1$$

$$\frac{\bar{q}'_{sq}}{\bar{q}'_t} \equiv 1$$

It is seen that the linear power output of the three lattices under natural circulation is the same for equal fuel volume fraction and equal pin diameters. This is a direct consequence of the fact that the hydraulic diameters are the same. It is also easily shown that power removal capabilities under forced convection laminar or turbulent flow conditions are also the same for the three lattices (see Appendix D).

In Chapter 4 some typical values of fluid and lattice

parameters will be used to calculate the pressure drops and mass flow rates for a range of linear power output. Using typical core and primary system parameter values, a $\bar{q}'$ for natural circulation will be calculated to see how this value compares to current linear power ratings for forced convection cooling.

Chapter 4

Example Calculations of Mass Flow Rate, Pressure Drop and Linear Power Output

4.1 Discussion

In Chapter 3 the relationships for the mass flow rate, the pressure drop, and the linear power output per cell were derived. In this chapter typical values for lattice parameters will be used to solve for the mass flow rate, the pressure drop, and linear power output for an open-hexagonal lattice and for a triangular lattice of equal fuel volume fraction, V_f', and equal pin diameter. As was seen in Chapter 3, the linear power output for triangular, open-hexagonal and square lattice arrangements are equal for equal fuel volume fraction, for equal core temperature drop, and for equal fluid properties in the three lattices. This equality is based on the condition that the pressure drop through the flow cells of the three lattices is equal since coolant velocities are equal in the three lattices. This condition is not strictly accurate because of the differences in the spacer arrangements. These differences introduce only small second order errors and can be neglected in a first order calculation of the relative linear power output. However, since they cannot be neglected in more precise calculations of the mass flow rate and linear power output of any given lattice arrangement, we will include calculations of these effects and tables of values of mass

flow rates, velocities and core pressure drop for a range of linear power output from one to twenty kilowatts per foot for the different lattices.

4.2 Calculation of Flow Parameters and Theoretical Spacer Pressure Drop in the Open-hexagonal Flow Cell

Refer to Figs. 1.1.a and 1.2.a for definition of the parameters required to calculate the expression for the V_f' of an open-hexagonal lattice. The values of the parameters used to calculate $(V_f')_h$ are $d_p = 0.300$ in., $\delta_h = 0.040$ in., and $p_h = 0.340$ in., from which

$$(V_f')_h = \frac{\pi\sqrt{3}}{9}\left(\frac{d_p}{p_h}\right)^2 = 0.472 \ . \qquad (4\text{-}1)$$

The value for d_p is about as large a value as is being considered for present LMFBR's fueled with uranium dioxide. The value for δ_h is about as small a pin to pin spacing as is being considered.

The following values will be used in calculating mass flow rates, pressure drop, and linear power output for an open-hexagonal lattice flow cell:

n_r = number of pins per cell = 2,

A_p = cross sectional area of a fuel pin = $\pi d_p^2/4$ = 0.00049 ft^2,

d_s = assumed spacer web thickness = 0.00125 ft,

n_s = number of spacer segments per cell = 9

l_s = length of one spacer segment = $p_h\sqrt{3}/3$ = 0.0164 ft,

A_s = cross sectional area of spacers per cell = $n_s l_s d_s$
= 0.000184 ft^2,

A_T = total cross sectional area of cell = $3\sqrt{3}p_h^2/2$
= 0.00209 ft^2,

A_1 = flow area away from the gridded region = $A_T - n_r A_p$
= 0.0011 ft^2,

A_2 = flow area in the gridded region = $A_1 - A_s$
=0.000918 ft^2 (see Fig. 3.2 for definition of flow regions),

$\sigma = A_2/A_1 = 0.834$.

Equation (3-11) can now be used to calculate the variation of flow rate with power output,

$$\bar{\omega} = \left(\frac{g\beta\rho^2 Z_e D_e^{1.2} S^{1.8} n_r \bar{q}'l}{0.092\mu^{0.2} N_e c_p f_s}\right)^{0.357}, \qquad (3\text{-}11)$$

with the following additional constants:

g = 4.16 x 10^8 ft/hr^2,

β = 1.6 x 10^{-4} $^oF^{-1}$,

ρ = 50 lb/ft^3,

μ = 0.5 lb/ft-hr,

c_p = 0.3 BTU/lb-^oF,

(Z_e/N_e) = 0.5,

D_e = $(3\sqrt{3}p_h^2 - \pi d_p^2)/\pi d_p$ = 0.0281 ft,

S = A_1 = 0.0011 ft^2,

n_r = 2 rods,

l = 4 ft,

f_s = 1 (see Eq. (3-10) for a definition of f_s).

Thus, for example, for $\bar{q}' = 10$ kw/ft = 34130 BTU/hr-ft, the average mass flow rate for an open-hexagonal lattice flow cell is $\bar{\omega} = 602$ lb/hr. Table IV.1 lists values of mass flow rate, coolant velocity in the ungridded region of a flow cell and corresponding Reynolds number for the open-hexagonal lattice. The coolant flow is seen to be turbulent for the range of linear power output considered.

The following computations are sample calculations of the average coolant velocities in and away from the gridded region of an open-hexagonal flow cell for the $\bar{q}' = 10$ kw/ft case. These velocities will be used in finding the pressure drop due to the fuel pins and the spacers in the open-hexagonal flow cell. The quantity $\bar{V}_1$ is the average coolant velocity away from the gridded region:

$$(\bar{V}_1)_h = \bar{\omega}/\rho(A_1)_h = 10{,}966 \text{ ft/hr} .$$

The quantity $\bar{V}_2$ is the average coolant velocity in the gridded region:

$$(\bar{V}_2)_h = \bar{\omega}/\rho(A_2)_h = 13{,}164 \text{ ft/hr} .$$

The quantity Re_1 is the Reynolds number for the coolant away from the gridded region:

$$(Re_1)_h = D_e\rho(\bar{V}_1)_h/\mu = 30{,}815 .$$

The quantity Re_2 is the Reynolds number for the coolant in the gridded region:

Table IV.1

Flow Parameters for the Open-hexagonal Lattice

$\bar{q}'$ (kw/ft)	$\bar{\omega}$ (lb/hr)	$\bar{V}_1$ (ft/hr)	Re_1
1	265	4,820	13,544
2	340	6,173	17,347
3	392	7,135	20,049
4	435	7,906	22,217
5	471	8,562	24,060
6	503	9,138	25,678
7	531	9,655	27,130
8	557	10,126	28,455
9	581	10,561	29,677
10	604	10,966	30,815
11	624	11,346	31,881
12	644	11,704	32,887
13	662	12,043	33,840
14	680	12,366	34,748
15	697	12,674	35,614
16	713	12,969	36,444
17	729	13,253	37,242
18	744	13,526	38,009
19	758	13,790	38,750
20	772	14,045	39,466

$$(Re_2)_h = D_e\rho(\bar{V}_2)_h/\mu = 36,990$$

From Fig. 3.3 for $\sigma = 0.834$, $K_c = 0.14$ and $K_e = -0.02$. Using Eqs. (3-3) and (3-6), the value for the total flow cell pressure drop is calculated:

$$(\Delta P_T - \Delta P_E) = \Delta P_R \frac{f}{Rf_{cir}} + \Delta P_s \qquad (3\text{-}3)$$

$$(\Delta P_T - \Delta P_E) = \frac{0.092\mu^{0.2}l\rho^{0.8}V_1^{1.8}}{D_e^{1.2}g_c}\left(\frac{f}{f_{cir}}\right) +$$

$$\frac{\rho(A_1/A_2)^2V_1^2}{2g_c}(K_e + K_c)n_g \qquad (3\text{-}6)$$

$$(\Delta P_T - \Delta P_E)_h = 1.28 \times 10^{-6}V_1^{1.8}(1.02) + 0.052 \times 10^{-6}V_1^2$$

$$(\Delta P_T - \Delta P_E)_h = 30.7 \text{ lb/ft}^2 .$$

Table IV.2 lists values of ΔP_R, $(\Delta P_R \frac{f}{Rf_{cir}})_h$, $((\Delta P_s)_{th})_h$, and $(\Delta P_T - \Delta P_E)_h$ for a range of linear power output. Since Reynolds numbers and velocities are equal for triangular and open-hexagonal lattices, ΔP_R's will be equal for the two lattices.

4.3 Calculations of Flow Parameters and Theoretical Spacer Pressure Drop in the Triangular Flow Cell

Refer to Figs. 1.1.b and 1.2.b for definition of the parameters required to calculate the expression for the V_f'

Table IV.2

Pressure Drop in the Open-hexagonal Lattice Flow Cell

$\overline{V}_1$ (ft/hr)	ΔP_R (lb/ft^2)	$\Delta P_R f/f_{cir}$ (lb/ft^2)	$((\Delta P_s)_{th})_h$ (lb/ft^2)	$(\Delta P_T - \Delta P_E)_h$ (lb/ft^2)
4,820	5.45	5.56	1.21	6.77
6,173	8.51	8.68	1.98	10.67
7,135	11.05	11.27	2.65	13.90
7,906	13.29	13.56	3.25	16.80
8,562	15.34	15.65	3.81	19.46
9,138	17.25	17.59	4.34	21.94
9,655	19.04	19.43	4.85	24.27
10,126	20.75	21.16	5.33	26.50
10,561	22.38	22.83	5.80	28.63
10,966	23.95	24.43	6.25	30.68
11,346	25.46	25.97	6.69	32.67
11,704	26.93	27.47	7.12	34.59
12,043	28.35	28.92	7.54	36.46
12,366	29.73	30.33	7.95	38.28
12,674	31.08	31.70	8.35	40.05
12,969	32.39	33.04	8.75	41.79
13,253	33.68	34.35	9.13	43.49
13,526	34.94	35.64	9.51	45.15
13,790	36.18	36.90	9.89	46.79
14,045	37.39	38.14	10.26	48.39

of a triangular lattice. Using the same fuel volume fraction and fuel pin diameter as were used for the open-hexagonal lattice,

$$(V_f')_t = \frac{\pi}{2\sqrt{3}}\left(\frac{d_p}{p_t}\right)^2 = 0.472 \ . \qquad (4\text{-}2)$$

Solving for the pitch and the pin to pin spacing gives:

$p_t = 0.416$ in.

$\delta_t = 0.116$ in.

The following values will be used in calculating mass flow rates, pressure drop, and linear power output for a triangular lattice flow cell:

$n_r = 1/2$,

$A_p = 0.00049$ ft^2,

$d_s = 0.00125$ ft,

$n_s = 1.5$,

$l_s = 0.02$ ft,

$A_s = 0.0000375$ ft^2,

$A_T = \sqrt{3}p_t^2/4 = 0.00052$ ft^2,

$A_1 = 0.000275$ ft^2,

$A_2 = 0.000237$ ft^2 (see Fig. 3.2 for definition of flow regions),

$\sigma = A_2/A_1 = 0.865$.

Equation (3-11) can again be used together with the following additional constants:

$g = 4.16 \times 10^8$ ft/hr^2,

$\beta = 1.6 \times 10^{-4}$ $^oF^{-1}$,

ρ = 50 lb/ft^3,

μ = 0.5 lb/ft-hr,

c_p = 0.3 BTU/lb-^oF,

(Z_e/N_e) = 0.5,

D_e = $(2\sqrt{3}p_t^2 - \pi d_p^2)/\pi d_p$ = 0.0281 ft,

S = A_1 = 0.000274 ft^2,

n_r = 1/2,

l = 4 ft,

f_s = 1.

Thus, for example, for $\bar{q}'$ = 10 kw/ft = 34130 BTU/hr-ft, the average mass flow rate for a triangular lattice flow cell is $\bar{\omega}$ = 150.5 lb/hr.

Table IV.3 lists values of mass flow rate, coolant velocity away from the gridded region, and the corresponding Reynolds number for the triangular lattice. Note that the corresponding coolant velocities and Reynolds numbers are the same for the open-hexagonal lattice since the fuel volume fractions are equal. Note also that the mass flow rates for the triangular lattice flow cell are one fourth of the corresponding mass flow rates for an open-hexagonal lattice flow cell. The differences are due to the differences in flow area, A_1, per cell and in the number of effective fuel rods, n_r, per cell. The mass flow rates per unit flow area, $\bar{\omega}/A_{cell}$, are equal for the two lattices.

The following computations are sample calculations of the average coolant velocities in and away from the gridded

Table IV.3

Flow Parameters for the Triangular Lattice

$\bar{q}'$ (kw/ft)	$\bar{\omega}$ (lb/hr)	$\bar{V}_1$ (ft/hr)	Re_1
1	66	4,820	13,544
2	85	6,173	17,347
3	98	7,135	20,049
4	108	7,906	22,217
5	118	8,562	24,060
6	125	9,138	25,678
7	132	9,655	27,130
8	139	10,126	28,455
9	145	10,561	29,677
10	150	10,966	30,815
11	155	11,346	31,881
12	161	11,704	32,887
13	165	12,043	33,840
14	170	12,366	34,748
15	174	12,674	35,614
16	178	12,969	36,444
17	182	13,253	37,242
18	186	13,526	38,009
19	189	13,790	38,750
20	193	14,045	39,466

region of a triangular flow cell for the $\bar{q}' = 10$ kw/ft case. These velocities will be used in finding the pressure drop due to the fuel pins and the spacers in the triangular lattice flow cell. The procedure is the same as that used in finding the pressure drop in the open-hexagonal lattice flow cell in Section 4.2.

$$(\bar{V}_1)_t = \bar{\omega}/\rho(A_1)_t = 10{,}966 \text{ ft/hr},$$

$$(\bar{V}_2)_t = \bar{\omega}/\rho(A_2)_t = 12{,}701 \text{ ft/hr}.$$

Note that $(\bar{V}_1)_t = (\bar{V}_1)_h$ since the fuel volume fractions are equal, but $(\bar{V}_2)_t$ is slightly less than $(\bar{V}_2)_h$ since the grid configurations are different for the two lattices.

$$(Re_1)_t = D_e\rho(\bar{V}_1)_t/\mu = 30{,}815$$

$$(Re_2)_t = D_e\rho(\bar{V}_2)_t/\mu = 35{,}688$$

From Fig. 3.3 for $\sigma = 0.865$, $K_c = 0.12$ and $K_e = -0.03$. Again using Eqs. (3-3) and (3-6), the value for the total flow cell pressure drop is calculated:

$$(\Delta P_T - \Delta P_E)_t = 1.28 \times 10^{-6}\bar{V}_1^{1.8}(1.095) + 0.036 \times 10^{-6}\bar{V}_1^2 ,$$

$$(\Delta P_T - \Delta P_E)_t = 30.54 \text{ lb/ft}^2 .$$

The lattice pressure drop $(\Delta P_T - \Delta P_E)_h$ and $(\Delta P_T - \Delta P_E)_t$ are very close in value. This is due to the offsetting effects of the values of the f/f_{cir} factors and the values

of the spacer pressure drop on the values of $(\Delta P_T - \Delta P_E)$ of the two lattices. Table IV.4 lists values of ΔP_R, $(\Delta P_{Rf}\frac{f}{f_{cir}})_t$, $((\Delta P_s)_{th})_t$, and $(\Delta P_T - \Delta P_E)$ for a range of linear power outputs.

4.4 Empirical Spacer Pressure Drop for the Triangular and Open-hexagonal Lattices

The method of de Stordeur for finding the empirical spacer pressure drop in a triangular lattice was presented in Section 3.4. Inserting the following values into Eq. (3-7), here repeated, and solving for $((\Delta P_s)_{em})_t$,

$$\Delta P_s = \frac{C_s V_s^2 S \rho}{2 g A_1}, \qquad (3\text{-}7)$$

$g = 4.16 \times 10^8$ ft/hr^2,

$A_1 = 0.000274$ ft^2,

$V_s = \bar{V}_2 = 12{,}687$ ft/hr,

$S = A_s = 0.0000375$ ft^2,

$\rho = 50$ lb/ft^3,

$C_s = 2.33$ (see Fig. 3.4 where $Re_s = d_s V_s \rho/\mu = 1{,}586$),

gives

$$((\Delta P_s)_{em})_t = 3.08 \text{ lb/ft}^2\text{-grid}.$$

Using the theoretical spacer pressure drop calculated for a triangular lattice in Section 4.3:

$$((\Delta P_s)_{th})_t = \frac{4.34 \text{ lb/ft}^2}{5 \text{ grids}} = 0.868 \text{ lb/ft}^2\text{-grid}.$$

Table IV.4

Pressure Drop in the Triangular Lattice Flow Cell

$\bar{V}_1$ (ft/hr)	ΔP_R (lb/ft^2)	$\Delta P_R f/f_{cir}$ (lb/ft^2)	$((\Delta P_s)_{th})_t$ (lb/ft^2)	$(\Delta P_T - \Delta P_E)_t$ (lb/ft^2)
4,820	5.45	5.97	0.84	6.80
6,173	8.51	9.32	1.37	10.69
7,135	11.05	12.10	1.84	13.93
7,906	13.29	14.55	2.25	16.80
8,562	15.34	16.80	2.64	19.44
9,138	17.25	18.89	3.00	21.90
9,655	19.04	20.85	3.36	24.20
10,126	20.75	22.72	3.69	26.41
10,561	22.38	24.51	4.02	28.52
10,966	23.95	26.23	4.34	30.57
11,346	25.46	27.88	4.64	32.51
11,704	26.93	29.49	4.93	34.42
12,043	28.35	31.04	5.22	36.26
12,366	29.73	32.55	5.50	38.06
12,674	31.08	34.03	5.78	39.81
12,969	32.39	35.47	6.06	41.53
13,253	33.68	36.88	6.32	43.20
13,526	34.94	38.26	6.58	44.84
13,790	36.18	39.62	6.84	46.46
14,045	37.39	40.94	7.10	48.04

Therefore,

$$((\Delta P_s)_{em})_h = \left(\frac{(\Delta P_s)_{em}}{(\Delta P_s)_{th}}\right)_t ((\Delta P_s)_{th})_h = 3.56((\Delta P_s)_{th})_h \ .$$

The pressure drop for the open-hexagonal lattice is

$$(\Delta P_T - \Delta P_E)_h = \frac{0.092\mu^{0.2}{}_1\rho^{0.8}\bar{V}_1^{1.8}}{D_e^{1.2}g_c}\left(\frac{f}{f_{cir}}\right)$$

$$+ \left(\frac{(\Delta P_s)_{em}}{(\Delta P_s)_{th}}\right)_t \frac{\rho(A_1/A_2)^2\bar{V}_1^2}{2g_c}(K_e + K_c)n_g \ ,$$

$$(\Delta P_T - \Delta P_E)_h = 24.4 + 3.59(6.25) = 46.8 \text{ lb/ft}^2.$$

Calculating the factor, f_s, gives (see Eq. (3-10)):

$$(f_s)_h = \frac{\Delta P_R f/f_{cir} + (\Delta P_s)_{em}}{\Delta P_R} = 1.96 \ .$$

Table IV.5 lists values of V_s, Re_s, C_s, $((\Delta P_s)_{em})_t$, $((\Delta P_s)_{th})_t$, $((\Delta P_s)_{em}/(\Delta P_s)_{th})_t$, and $((\Delta P_s)_{em})_h$ used in finding $(f_s)_h$ for a range of linear power output from one to twenty kilowatts per foot. $(\Delta P_R)_h$ and $(\Delta P_R f/f_{cir})_h$ are found in Table IV.2. The factor $(f_s)_h$ is relatively constant, with an average value of 1.95. The quantity $(\Delta P_T - \Delta P_E)_h = (\Delta P_R f_s)_h$ is also tabulated in Table IV.5.

For more accurate pressure drop calculations, $(f_s)_h$ should be used in Eq. (A-8) for finding the mass flow rate

Table IV.5

Flow Parameters and Pressure Drop in the Spacer Region for the Triangular Lattice Flow Cell

$\bar{q}'$ (kw/ft)	V_s (ft/hr)	Re_s ---	C_s ---	$((\Delta P_s)_{em})_t$ lb/ft^2-grid
1	5,577	697	2.68	0.68
2	7,142	893	2.56	1.07
3	8,255	1,032	2.51	1.41
4	9,147	1,143	2.47	1.70
5	9,906	1,238	2.44	1.97
6	10,573	1,322	2.41	2.21
7	11,171	1,396	2.39	2.45
8	11,716	1,464	2.38	2.69
9	12,219	1,527	2.36	2.90
10	12,687	1,586	2.35	3.11
11	13,127	1,641	2.34	3.31
12	13,542	1,693	2.33	3.51
13	13,934	1,742	2.32	3.70
14	14,307	1,788	2.31	3.89
15	14,664	1,833	2.30	4.07
16	15,005	1,876	2.29	4.24
17	15,334	1,917	2.28	4.41
18	15,650	1,956	2.27	4.57
19	15,955	1,994	2.26	4.73
20	16,250	2,031	2.25	4.91

Table IV.5 continued

$((\Delta P_s)_{th})_t$ (lb/ft^2)	$\left(\frac{(\Delta P_s)_{em}}{(\Delta P_s)_{th}}\right)_t$	$((\Delta P_s)_{em})_h$ lb/ft^2-grid	$(f_s)_h$ ---	$(\Delta P_R f_s)_h$ (lb/ft^2)
0.84	4.10	4.96	1.93	10.63
1.37	3.92	7.76	1.93	16.59
1.84	3.83	10.15	1.94	21.55
2.25	3.78	12.27	1.94	25.92
2.64	3.73	14.20	1.95	29.90
3.00	3.68	15.99	1.95	33.64
3.36	3.65	17.72	1.95	37.13
3.69	3.64	19.39	1.95	40.46
4.02	3.61	20.92	1.95	43.64
4.34	3.59	22.44	1.96	46.70
4.64	3.58	23.92	1.96	49.65
4.93	3.56	25.36	1.96	52.51
5.22	3.55	26.74	1.96	55.28
5.50	3.53	28.07	1.96	57.97
5.78	3.51	29.34	1.96	60.60
6.06	3.59	30.62	1.97	63.16
6.32	3.48	31.80	1.96	65.68
6.58	3.47	33.00	1.96	68.13
6.84	3.45	34.16	1.96	70.55
7.10	3.45	35.44	1.97	72.91

of the open-hexagonal lattice flow cell. Coolant velocities and cell and spacer pressure drop would be recomputed to find a corrected $(f_s)_h$. This process would be continued until succeeding $(f_s)_h$'s were essentially constant.

The factor, f_s, for the triangular lattice is calculated by the same procedure as was used to calculate $(f_s)_h$. The average value of $(f_s)_t$ is 1.74. The factor, $(f_s)_t$, is not equal to $(f_s)_h$ since the spacer pressure drop in the two lattices are different, a condition due to the difference in spacer configuration in the two lattices.

4.5 Linear Power Output for the Open-hexagonal Lattice

Using Eq. (3-13),

$$\bar{q}' = \left(\frac{g\beta\rho^2 Z_e D_e^{1.2} S^{1.8} n_r}{0.092\mu^{0.2} N_e f_s}\right)^{0.555} \left(\frac{\Delta t}{n_r}\right)^{1.555} \left(\frac{c_p}{l}\right)^{1.0}, \qquad (3\text{-}13)$$

the average linear power for the open-hexagonal lattice is calculated using the following constants:

$g = 4.16 \times 10^8$ ft/hr^2,

$\beta = 1.6 \times 10^{-4}$ $^\circ$F^{-1},

$\rho = 50$ lb/ft^3,

$\mu = 0.5$ lb/ft-hr,

$c_p = 0.3$ BTU/lb/$^\circ$F,

1 kw = 3413 BTU/hr .

In terms of several system variables, the linear power output can be expressed as

$$\bar{q}' = 22.4\left(\left(\frac{Z_e}{N_e}\right)^{0.555}\left(\frac{1}{f_s}\right)^{0.555}\left(\frac{\Delta t}{100}\right)^{1.555} D_e^{0.666}\left(\frac{S}{n_r l}\right)^{1.0}\right) , \quad (4\text{-}3)$$

where Δt is in $^{\circ}F$, D_e is in inches, S is in square inches, and l is in feet. Inserting the following typical values into Eq. (4-3):

Z_e/N_e = 0.5 (i. e., the ratio of the source/sink elevation difference and the effective primary circuit length),

Δt = 400 $^{\circ}F$,

S = 0.1587 $in.^2$ (the cross sectional flow area for the open-hexagonal flow cell in these calculations),

f_s = 1.95,

D_e = 0.337 in. (the equivalent diameter for the open-hexagonal flow cell in these calculations),

n_r = 2 rods,

l = 4 ft,

the average linear power output for the open-hexagonal lattice (and for the triangular and square lattices) is

$$\bar{q}'_h = 0.873 \text{ kw/ft} .$$

The above value for $\bar{q}'$ is low compared to the required full power output of a practical reactor, which averages around 10 kw/ft. On the other hand, 8.73% of full power is a respectable rating in terms of decay heat removal. Suggestions for increasing the value of the linear power output achievable with natural circulation flow are made in Chapter 6.

The mass flow rates, $\bar{\omega}$, coolant velocities, $\bar{V}$, and friction pressure drop, ΔP_R, calculated in the preceding example were based on an $f_s = 1$. Table IV.6 lists the mass flow rates per unit flow area, $\bar{\omega}/A_{cell}$, and the total friction pressure drop, $\Delta P_R f_s$, calculated using $(f_s)_h = 1.95$ and $(f_s)_t = 1.74$ in Eq. (3-11). The tube bundle friction pressure drop, ΔP_R, was calculated from

$$\Delta P_R = 1.28 \times 10^{-6} \bar{V}_1^{1.8} \text{ lb/ft}^2 ,$$

where

$$\bar{V}_1 = \frac{\bar{\omega}}{\rho A_1} .$$

Figure 4.1 shows the natural circulation operating conditions for the open-hexagonal and triangular lattices. Using a $\Delta t = 400\ ^{\circ}F$, the linear power output of the two lattices vary by the factor $(1/f_s)^{0.357}$. Since $(A_{cell})_h = 4(A_{cell})_t$ and $\bar{\omega}_h \approx 4\bar{\omega}_t$, the horizontal axis of Fig. 4.1 is in units of $\bar{\omega}/A_{cell}$ for ease of comparison of the performance of the two lattices. Figure 4.1, which is based on the values in Table IV.6, shows that for equal total friction pressure drop and equal Δt, the triangular lattice has a slightly higher linear power output than does the open-hexagonal lattice.

Table IV.6

Mass Flow Rates per Unit Flow Area and Total Friction Pressure Drop as Functions of a Calculated f_s in the Open-hexagonal and Triangular Flow Cells

$\bar{q}'$ (kw/ft)	$(\bar{\omega}/A_{cell})_h$ (lb/hr-ft^2)	$(\Delta P_R f_s)_h$ (lb/ft^2)	$(\bar{\omega}/A_{cell})_t$ (lb/hr-ft^2)	$(\Delta P_R f_s)_t$ (lb/ft^2)
1	190,000	6.9	198,000	6.6
2	243,500	10.8	253,500	10.4
3	281,000	14.0	292,500	13.5
4	311,500	16.8	324,500	16.2
5	337,500	19.4	351,500	18.7
6	360,500	21.8	375,000	21.1
7	380,500	24.1	396,000	23.2
8	399,000	26.3	415,500	25.3
9	416,000	28.4	433,500	27.3
10	432,500	30.4	450,500	29.2

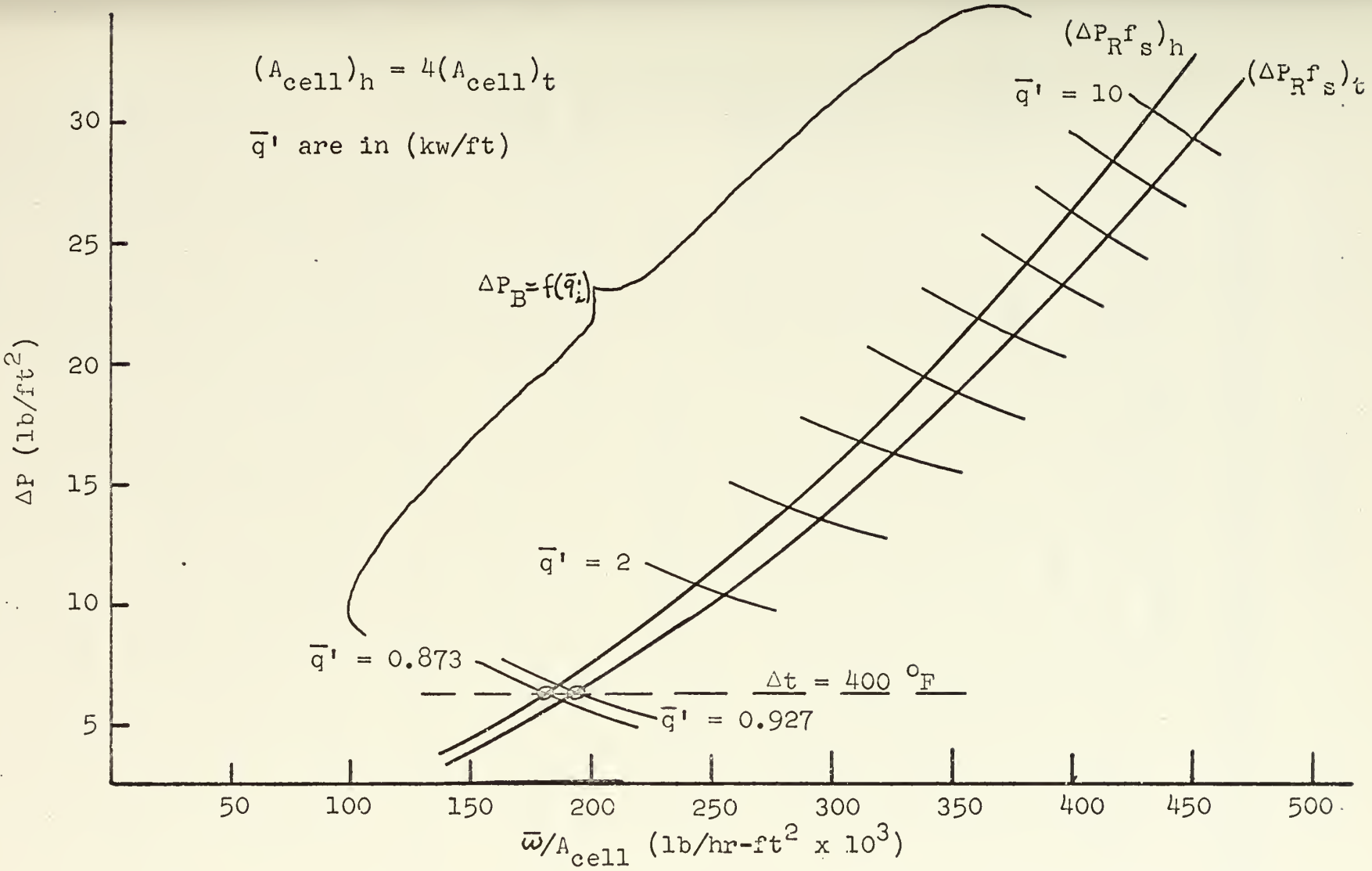

Fig. 4.1. Natural circulation operating conditions denoted by ⊙ for the open-hexagonal and triangular lattices.

Chapter 5

Equivalent Diameter for the Open-hexagonal Lattice

5.1 Definition of Equivalent Diameter

Whenever flow in noncircular ducts is considered, it is necessary to employ in the calculation of the Reynolds number and friction factor some characteristic dimension. In circular ducts the characteristic dimension is the diameter, D. In noncircular ducts the concept of equivalent diameter, D_e, (also referred to as hydraulic diameter) applies when the duct does not appreciably vary from circular. The equivalent diameter is defined as

$$D_e = \frac{4 \times \text{cross sectional flow area}}{\text{wetted perimeter}} = \frac{4A}{P_w} \quad . \qquad (5\text{-}1)$$

The equivalent diameter is the characteristic length which would give the same ratio of fluid passage volume to wetted area for circular and noncircular ducts.

5.2 Conditions for a Laminar Flow Region in the Open-hexagonal Flow Cell

In a noncircular duct the concept of equivalent diameter applies for turbulent or laminar flow. However, the values for the Reynolds number and friction factor are different for laminar and turbulent flow. In a unit open-hexagonal cell (refer to Fig. 1.2.a) the flow passage is approximately circular; therefore, the concept of equivalent

diameter should apply. In Chapter 4 the Reynolds number and friction factor for the open-hexagonal cell were calculated assuming fully turbulent flow in all parts of the cell. These numbers were computed using the average cell rate of flow which was turbulent. For turbulent flow

$$f_F = 0.046 Re^{-0.2} \quad .$$

However, it is possible that the flow is laminar in some sections of the flow cell, namely, in the narrow flow area between two adjacent fuel pins. If this is the case, then the Reynolds number and friction factor are different in the laminar flow area from the Reynolds number and friction factor in the rest of the flow area. For laminar flow

$$f_F = 16 Re^{-1} \quad .$$

In order to determine if the flow in the region between adjacent fuel pins is fully laminar, a rough calculation of the laminar sub-layer thickness around the fuel pins will be made. The pin to pin spacing is 0.040 inches; therefore, if the laminar sub-layer around each pin is as much as 0.020 inches, the region may be considered to have laminar flow. If this be the case, the open-hexagonal flow cell can be divided into two channels, one having turbulent flow and one having laminar flow. This division of the flow cell assumes no inter-channel mixing and little or no heat transfer from the laminar region to the turbulent region. This

assumption is not good if there is a significant degree of inter-channel coolant mixing, which in fact probably occurs in the present case since the channels are not isolated. This assumption breaks down also if the heat transfer from channel to channel is good.

If it is found that open-hexagonal cells can be divided into two channels, the coolant flow rates would have to be recomputed using two flow regions per cell in order that the power output could be recomputed. Since the pressure drop through the subassembly, ΔP_{SA}, will be the same for all flow regions, the coolant velocity in the laminar channel will be less than the coolant velocity in the turbulent channel in accordance with:

$$(\Delta P_{SA})_{Lam} = (\Delta P_{SA})_{Tur} \quad ,$$

$$(4f\frac{L\rho V^2}{D_e 2})_{Lam} = (4f\frac{L\rho V^2}{D_e 2})_{Tur} \quad .$$

From this last relation it follows that

$$V_{Lam} < V_{Tur} \quad , \qquad (5\text{-}2)$$

since the friction factor for fully laminar flow is greater than the friction factor for fully turbulent flow in a smooth pipe or duct, and the laminar region D_e is approximately less than or equal to the turbulent region D_e. Calculations of the equivalent diameters for the two regions showed $(D_e)_{Lam} \leq (D_e)_{Tur}$ in the open-hexagonal flow cell.

Since $V_{Lam} < V_{Tur}$, then $\omega_{Lam} < \omega_{Tur}$, where ω_{Lam} is the mass flow rate in the laminar channel of the flow cell, and ω_{Tur} is the mass flow rate in the turbulent channel of the flow cell. If it is desired to maintain the core Δt at a certain amount, then $(\omega_{Lam} + \omega_{Tur}) < \omega_{sr}$ where ω_{sr} is the flow rate based on a single region of fully turbulent flow in the entire flow cell. The sum of ω_{Lam} and ω_{Tur} is less than ω_{sr} because ω_{Lam} in the laminar channel is less than ω_{Tur}. Since c_p and Δt are constant and $(\omega_{Lam} + \omega_{Tur}) < \omega_{sr}$, then $\bar{q}_{Tot}$ will have to be decreased from the value calculated in a single region (turbulent) flow correlation $(\bar{q}_{Tot})_{sr} = \omega_{sr} c_p \Delta t$, thus degrading the power output of the entire core.

5.3 Calculation of Laminar Sub-layer Thickness in Turbulent Flow

The thickness of the laminar sub-layer around the fuel pins will be calculated to a first order approximation using equations given by Schlichting[12]. The laminar momentum sub-layer thickness, δ_l, for turbulent flow in pipes is given by Schlichting's Eq. (20.15a) as

$$\delta_l \approx \frac{\nu}{\bar{v}_*} \quad . \tag{5-3}$$

The friction velocity, v_*, is given by his Eq. (20.8) as

$$v_* = (T_o/\rho)^{1/2} = (0.03955 \bar{\mu}^{-7/4} \nu^{1/4} d^{-1/4})^{1/2} \quad , \tag{5-4}$$

where

T_o is the shear stress at the wall,

$\bar{u}$ is the average velocity in the pipe,

ν is the kinematic fiscosity of the fluid,

d is the pipe diameter.

Using the following values from the example calculations in Chapter 4:

$d = (D_e)_h = 0.0281$ ft

$\bar{u} = \bar{V}_1 = 10{,}966$ ft/hr

$\nu = \mu/\rho = 0.01$ ft^2/hr

the friction velocity is $v_* = 598$ ft/hr, and the laminar momentum sub-layer thickness $\delta_1 \approx 0.001$ in. The thermal boundary layer thickness on the other hand is $\delta_{th} \approx k/h$. Using the following approximate values for liquid sodium:

$k = 40$ BTU/hr-ft-°F,

$h = 20{,}000$ BTU/hr-ft^2-°F,

the thermal boundary layer is $\delta_{th} \approx 0.002$ in.

These values of δ_1 and δ_{th} are considerably less than 0.020 inches, the value necessary to establish a laminar flow region between adjacent fuel pins. Therefore, the flow in all regions of the open-hexagonal flow cell can be considered to have turbulent flow. Consequently, the open-hexagonal flow cell can be considered to have only one flow region, and an equivalent diameter, defined by Eq. (5-1), can be calculated for the entire cell.

The above calculations of δ_1 and δ_{th} were only approximate. A more accurate computer calculation using a code

such as General Electric's Velvet-II Code[13] can be made of the velocity profiles around the fuel pins. However, there is no reason to expect that more sophisticated calculations would alter the above conclusions.

Chapter 6

Summary and Conclusions

6.1 Summary

The work reported in the preceding chapters has compared the open-hexagonal, triangular, and square lattice configurations under natural circulation flow with respect to leakage reactivity effects in a coolant cell upon sodium voiding, mass flow rate and pressure drop in the coolant channels, and linear power output. The basis for comparison of the three lattices was equal fuel rod size and volumetric composition in the cores. The open-hexagonal lattice was found to be preferable from the standpoint of leakage reactivity upon sodium voiding because of its larger coolant channel nuclear hydraulic radius. For the same cell bulk temperature rise the mass flow rates per cell flow area, $\bar{\omega}_{cell}/A_{cell}$, were found to be equal for the three lattice flow cells. The pressure drop through the lattices were approximately equal; the small differences in pressure drop were due to the differences in spacer configuration. The linear power outputs of the three lattices were found to be equal for the three lattices assuming equal core pressure drop. Example calculations of the above quantities were presented. It was also found that the fluid flow and heat transfer characteristics of the three lattices were equal under forced circulation for both laminar and turbulent flow. Finally, the applicability of the equivalent diameter

concept for use in calculation of heat transfer and fluid flow characteristics of the open-hexagonal flow cell was examined. It was found that the conventional expression for equivalent diameter can be used for the open-hexagonal lattice.

6.2 Discussion

The open-hexagonal lattice was found to be superior to the triangular and square lattices with respect to leakage reactivity upon sodium voiding. If more sophisticated calculations confirm that the added negative leakage component of the sodium void reactivity effect in the open-hexagonal lattice is indeed several dollars, there would be a definite advantage from a safety standpoint in employing this lattice in either natural or forced convection LMFBR's.

However, from the standpoint of hydraulic and thermal performance examined in this study, the open-hexagonal lattice was not found to be superior to the triangular or square lattices in any way. The triangular lattice would, in fact, be preferable to an open-hexagonal lattice since more fuel pins can be packed into a given area of core while still maintaining prudent pin to pin spacings. Assuming the present FFTF pin spacing of 0.0625 inches for a triangular lattice and equal pin diameters of d_p = 0.300 inches for both lattices, the fuel pins in the open-hexagonal lattice would have to be touching per Eq. (B-1) in order to retain an equal fuel volume fraction in the two lattices. If a pin to pin spacing for the open-hexagonal lattice were to be held at 0.040 inches, the V_f as calculated in Appendix C

would have to be held to around 0.306 without considering stainless steel swelling and to 0.288 with consideration given to stainless steel swelling. Larger pin sizes for the open-hexagonal lattice would allow larger V_f, but the increase in V_f would not be significant if the pin to pin spacing was held at a reasonable value ($\delta_h < 0.020$ inches). This can be seen from the decreasing slope of the V_f' versus d_p curve of Fig. C.1. Current and future design values for V_f are found in Table C.1.

Since the natural convection performance of all three lattices is equal in the hydraulic and thermal aspects examined, improvements in the linear power output achieved by all three lattices can be suggested using Eq. (A-10),

$$\bar{q}' = \left(\frac{g\beta\rho^2 Z_e D_e^{1.2} S^{1.8} n_r}{0.092\mu^{0.2} N_e f_s}\right)^{0.555} \left(\frac{\Delta t}{n_r}\right)^{1.555} \left(\frac{c_p}{l}\right)^{1.0}. \qquad \text{(A-10)}$$

In Chapter 4 a value for Z_e/N_e, the ratio of the source/sink elevation difference and the effective primary circuit length, of 0.5 was employed. This ratio can be increased. Using values from the FFTF design proposals for a 400 Mwt LMFBR[14], a typical value for N_e is

$$N_e = \frac{\Delta P_{pump}}{\Delta P_{core}} L_{core} = 11.6 \text{ ft},$$

where

$$\Delta P_{pump} = 145 \text{ psi}$$

ΔP_{core} = 100 psi

L_{core} = 8 ft

By employing a Z_e of up to say 24 feet, the ratio Z_e/N_e could be made as large as 2.0. For a value of $Z_e/N_e = 2.0$, the linear power output calculated in Chapter 4 would be increased by a factor of $(2.0/0.5)^{0.555} = 2.16$. In Chapter 4 the value of the core temperature rise was 400 °F. If this value could be raised to 450 °F, the linear power output would be increased by a factor of $(450/400)^{1.555} = 1.2$. A core Δt of 400 °F is about as large a value as is practical. A larger value of Δt may produce a thermal shock upon reactor scram which the primary system could not withstand. The linear power output could also be increased by spacing the fuel pins farther apart while increasing pin diameter. The wider spacing would increase the equivalent diameter, D_e, and coolant flow area, S, thus increasing $\overline{q}'$ since $\overline{q}' = f((D_e^{1.2}S^{1.8})^{0.555}) = f(D_e^{0.666}S)$. The core temperature rise, Δt, would also increase with this change in spacing through the relation $\overline{q}'\eta_r l = \overline{q} = \overline{\omega} c_p \Delta t$. However, the spacing contribution probably would not increase $\overline{q}'$ by much. In Chapter 4 the core length, l, was four feet. The length l could possibly be reduced by as much as two feet, thus raising $\overline{q}'$ by the factor $(4/2)^{1.0} = 2$. Combining the above suggested contributions for increasing $\overline{q}'$ gives a total factor of about 5.2. With these contributions $\overline{q}'$ would equal 4.54 kw/ft instead of 0.873 kw/ft as calculated

in Chapter 4. However, 4.54 kw/ft is in reality a peak value for the natural circulation case. It is less than 50% of the desired 10 kw/ft average and less than 30% of the 16 kw/ft peak (assuming axial and radial peaking factors of about 1.25 and 1.26) needed to match projected 1000 Mwe forced convection plant operating conditions[15A]. Unless a better combination of the variables discussed above can be achieved, full power operation under natural circulation is not practical.

A summary of the parameters assumed and calculated in this study is presented in Table VI.1.

6.3 Future Work

Since the leakage reactivity effect in the open-hexagonal lattice provides a significant additional negative reactivity contribution compared to the triangular and square lattices, a more sophisticated calculation by Monte Carlo or other methods should be made to determine a precise value for the sodium void negative reactivity component in the open-hexagonal lattice. The model used in this study yielded only approximate answers under the assumption of an infinite core. An experiment measuring the relative and absolute negative reactivity of the lattices should also be considered. However, since the reactivity change is on the order of one percent of the effective multiplication factor, the necessary precision for measuring the reactivity change would be difficult to design into the experiment.

Table VI.1

Assumed and Calculated Core Parameters for Various Lattices

Item	Units	Source	Triangular	Open-hexagonal	Square
V_f'	ft^3/ft^3	App. C, Chap. 4	0.472 assumed	0.472 assumed	0.472 assumed
d	in.	App. C, Chap. 4	0.300 assumed	0.300 assumed	0.300 assumed
δ	in.	App. C	0.116	0.040 assumed	----
p	in.	App. C	0.416	0.340	----
n_r	rods	Fig. 1.1	1/2	2	1
D_e	ft	App. B, Chap. 4	0.0281	0.0281	0.0281
$S = A_1$	ft^2	Eqs. (D-4)-(D-6)	$A_h/4$	A_h =0.0011	$A_h/2$
$\bar{\omega} \propto (n_r S^{1.8})^{0.357}$	lb/hr	App. A, Chap. 4	$\bar{\omega}_h/4$	$\bar{\omega}_h$ = 602	----
$\bar{\omega}/A_{cell}$	$\frac{lb/hr}{ft^2}$	Chap. 4	547,000	547,000	547,000
$V=\frac{\bar{\omega}}{\rho S} \propto (\frac{n_r}{S})^{0.357}$	ft/hr	Chap. 4	10,966	10,966	10,966
$\Delta P_R=4f\frac{L\rho V^2}{FD_e 2g_c}$	lb/ft^2	Chap. 4	23.95	23.95	23.95
f_s	$\frac{lb/ft^2}{lb/ft^2}$	Eq. (3-10)	1.74	1.95	----

Models of the three lattices could be constructed to test the pressure drop performance of the different configurations. Freon or water could be used as the test coolant.

6.4 Conclusion

This study has shown that from hydraulic and thermal aspects, the triangular, open-hexagonal and square lattices are essentially equivalent under forced and natural circulation. For natural circulation operation it was shown that the linear power output of the three lattices was far less than the desired value for full power operation, even under an optimum combination of constraints. Therefore, nome of the lattices are practical for full power operation under natural circulation. Furthermore, unless the open-hexagonal lattice is found to contribute significantly to the negative component of the sodium void reactivity effect, the triangular lattice is preferable for forced convection operation.

Appendix A

Linear Power Relationship for Natural Circulation in a Reactor

If z is the elevation above a datum surface (see Fig. A.1) at which the pressure is constant, the difference in pressure between elevations z_2 and z_1 in a static fluid (no friction nor acceleration) is

$$P_2 - P_1 = \int_{z_2}^{z_1} \frac{\rho g dz}{g_c} = \frac{\bar{\rho} g (z_1 - z_2)}{g_c} . \qquad (A\text{-}1)$$

Integrating completely around a closed circuit which has the fluid in two legs at different densities gives

$$\Delta P_B = \frac{g}{g_c}\left(\int_{z_2}^{z_1} \rho_c dz + \int_{z_1}^{z_2} \rho_h dz\right),$$

$$\Delta P_B = \frac{g}{g_c} \int_{z_1}^{z_2} (\rho_h - \rho_c) dz .$$

Introducing the temperature coefficient of volumetric expansion, β:

$$\rho_h - \rho_c = \rho_c \beta_c (t_h - t_c) ,$$

$$\Delta P_B = \frac{g \rho_c \beta_c}{g_c} \int_{z_i}^{z_2} (t_h - t_c) dz . \qquad (A\text{-}2)$$

Using $\bar{q} = \bar{\omega} c_p (t_h - t_h)$ where $\bar{q}$ is the heat produced per

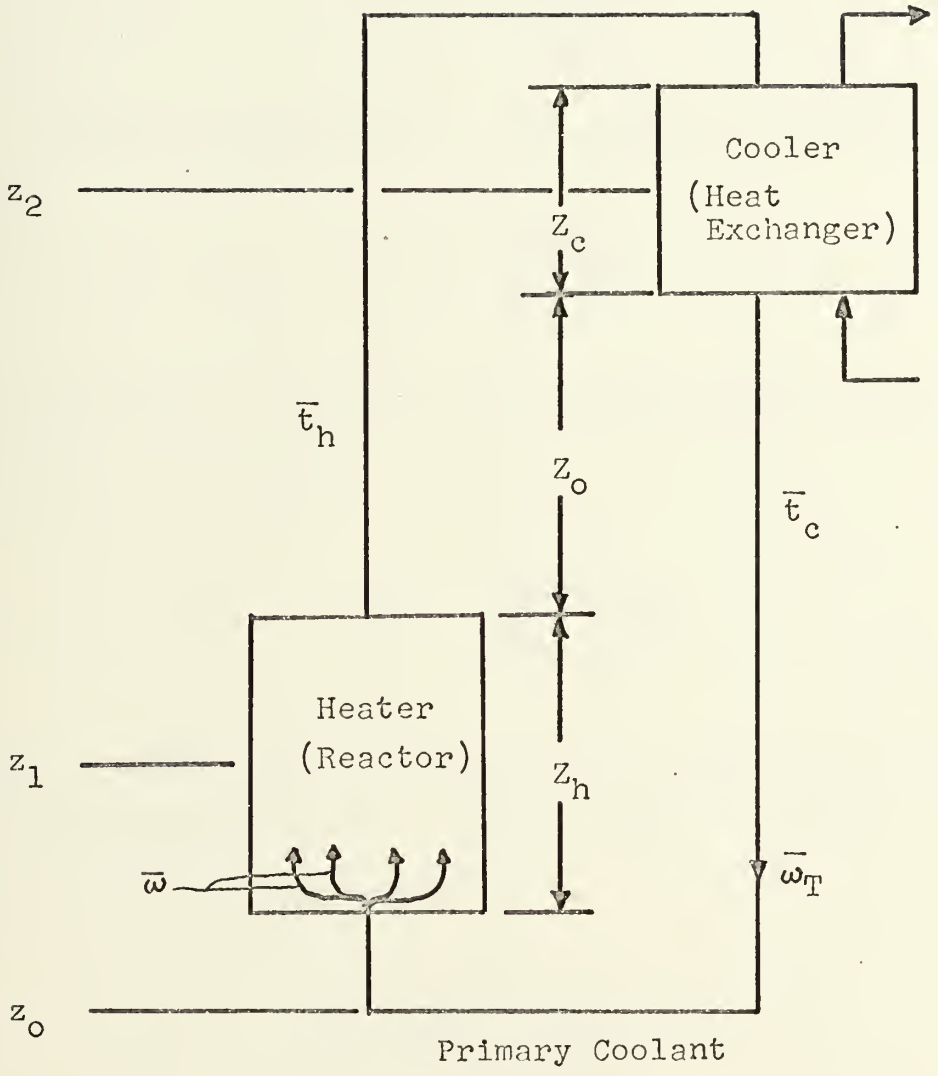

Fig. A.1. Thermal circulation driving heads.(16)

unit cell, and $\bar{\omega}$ is the mass flow rate per cell and $z_2 - z_1 = Z_e = Z_0 + (Z_c + Z_h)/2$,

$$\Delta P_B = \frac{g\beta_c \rho_c \bar{q} Z_e}{g_c c_p \bar{\omega}} \quad . \tag{A-3}$$

From the definition of the Fanning friction factor,

$$f_F = \frac{\Delta P_R g_c D}{2N_e \rho \bar{\omega}^2} \quad , \tag{A-4}$$

an expression for the friction pressure drop, ΔP_R, is obtained as follows:

$$\Delta P_R = \frac{2N_e \rho \bar{\omega}^2 f_F f_s}{g_c D_e \rho^2 S^2} \quad , \tag{A-5}$$

where f_s, the factor accounting for spacer pressure drop, is defined by Eq. (3-10), and $\bar{u} = \bar{\omega}/\rho S$. Equating ΔP_B and ΔP_R and solving for $\bar{\omega}$ gives

$$\bar{\omega} = \left(\frac{g\beta\rho^2 \bar{q} Z_e D_e S^2}{2N_e c_p f_F f_s}\right)^{1/3} \quad . \tag{A-6}$$

In this derivation N_e is the total effective length of the primary coolant system:

$$N_e = \frac{\Delta P_{pump} L_{core}}{\Delta P_{core}}$$

where L_{core} is the length of the core. The quantity N_e is a measure of the equivalent length of the complete primary circuit (core, pipes, and heat exchanger) expressed in terms of an extended core of height N_e and channel diameter D_e. Substituting the relationship $f_F = 0.046Re^{-0.2}$ $= 0.046\mu^{0.2}/(D_e\bar{\omega}/S)^{0.2}$ for turbulent flow into Eq. (A-6) gives

$$\bar{\omega} = \left(\frac{g\beta\rho^2 Z_e D_e^{1.2} S^{1.8} \bar{q}}{0.092\mu^{0.2} N_e c_p f_s}\right)^{0.357} . \qquad \text{(A-7)}$$

Using the relationships $\bar{q} = n_r \bar{q}' l$, where n_r is the number of effective fuel rods per unit cell, and $\bar{q} = \bar{\omega} c_p \Delta t$, where $\Delta t = t_h - t_c$:

$$q' = \frac{\bar{\omega} c_p \Delta t}{n_r l} . \qquad \text{(A-8)}$$

Substituting Eq. (A-7) into Eq. (A-8) yields

$$\bar{q}' = \left(\frac{g\beta\rho^2 Z_e D_e^{1.2} S^{1.8} n_r \bar{q}' l}{0.092\mu^{0.2} N_e c_p f_s}\right)^{0.357} \left(\frac{c_p \Delta t}{n_r l}\right) . \qquad \text{(A-9)}$$

Solving for $\bar{q}'$, Eq. (A-9) becomes

$$\bar{q}' = \left(\frac{g\beta\rho^2 Z_e D_e^{1.2} S^{1.8} n_r}{0.092\mu^{0.2} N_e f_s}\right)^{0.555} \left(\frac{\Delta t}{n_r}\right)^{1.555} \left(\frac{c_p}{l}\right)^{1.0} . \qquad \text{(A-10)}$$

Refer to Fig. 3.6, which is reproduced below as Fig. A.2, for the physical illustration of these results. Fig. A.3 shows a comparison of the driving forces in the forced and natural convection cases.

For natural convection the following observations are made: If it is desired to increase $\bar{q}'$, this is done by allowing an increase in Δt. This in effect increases the driving head allowing a greater flow rate, $\bar{\omega}$ per Eq. (A-8) at which the $\Delta P_B = \Delta P_R$. The combination of an increase in both Δt and $\bar{\omega}$ increases $\bar{q}$ according to the relation $\bar{q} = \bar{\omega} c_p (t_h - t_c)$, and thereby $\bar{q}'$ increases for fixed n_r and l, since $\bar{q}' = \bar{q}/n_r l$.

Note if Δt is fixed, i. e., a maximum allowable core temperature drop is specified, the cell operating condition for constant cell parameters n_r and l is fixed at the intersection of the three lines Δt, ΔP_R, and ΔP_B. This intersection fixes $\bar{\omega}$ and hence $\bar{q}$ and $\bar{q}'$ through $\bar{q} = \bar{\omega}_{fixed} c_p (t_h - t_c)_{fixed}$ and $\bar{q}' = \bar{q}/n_r l = \bar{\omega} c_p \Delta t / n_r l$ from Eq. (A-10).

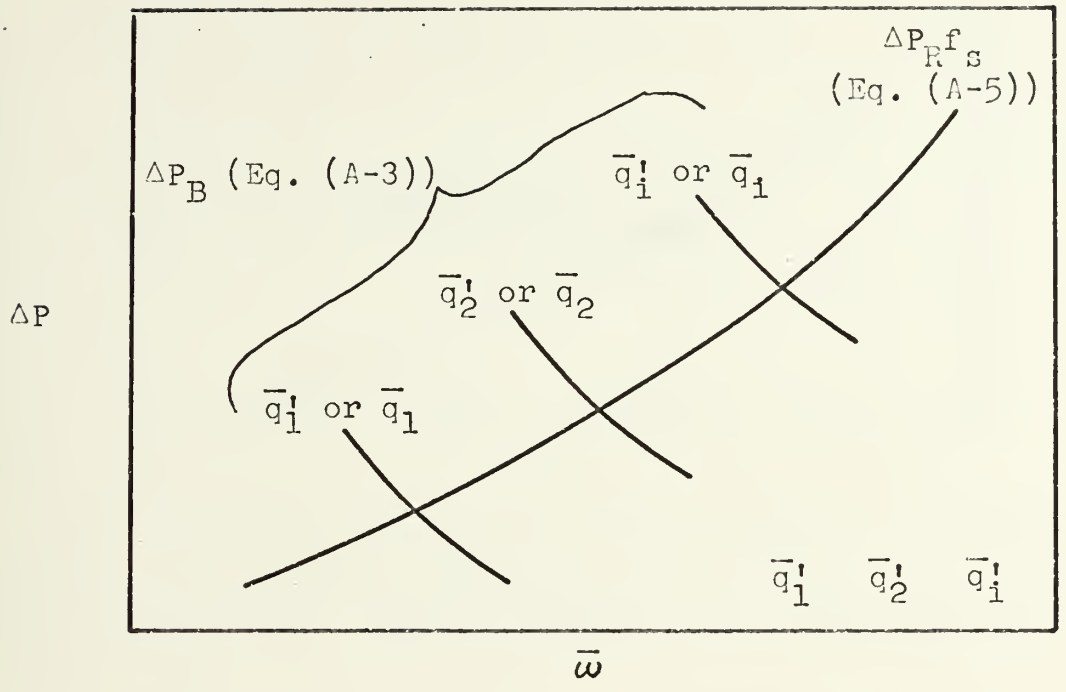

a. Intersection points given by Eq. (A-7).

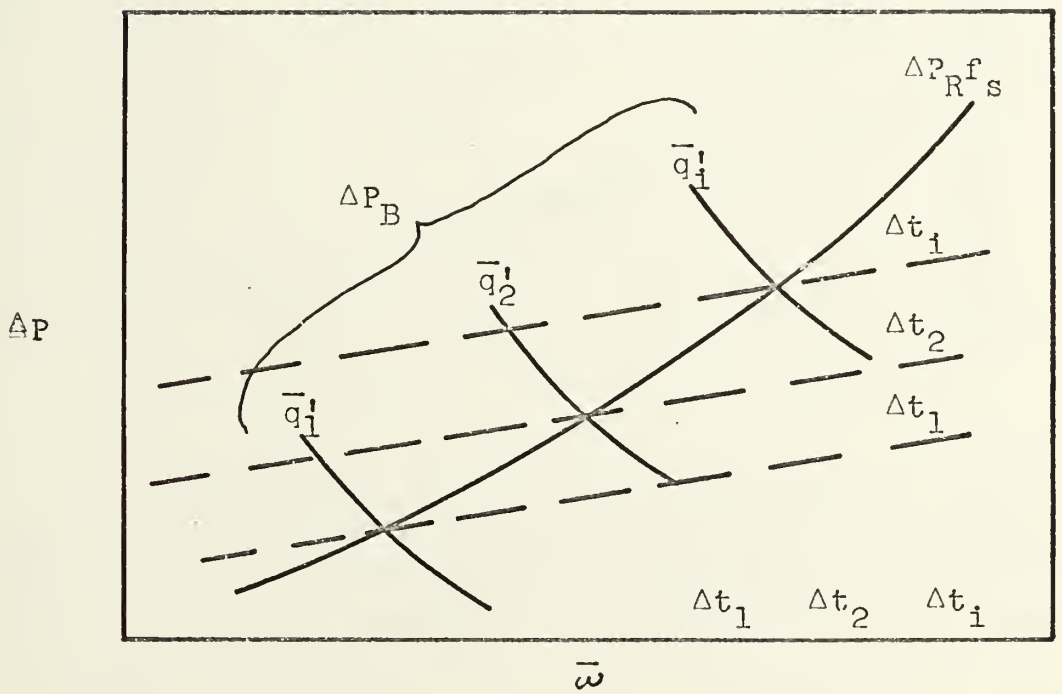

b. Eq. (A-10) yields the $\bar{q}'$ which corresponds to the intersection points of the three lines; i. e., for conditions of $\Delta P_B = \Delta P_R$ and Δt fixed.

Fig. A.2. Natural circulation operating conditions.

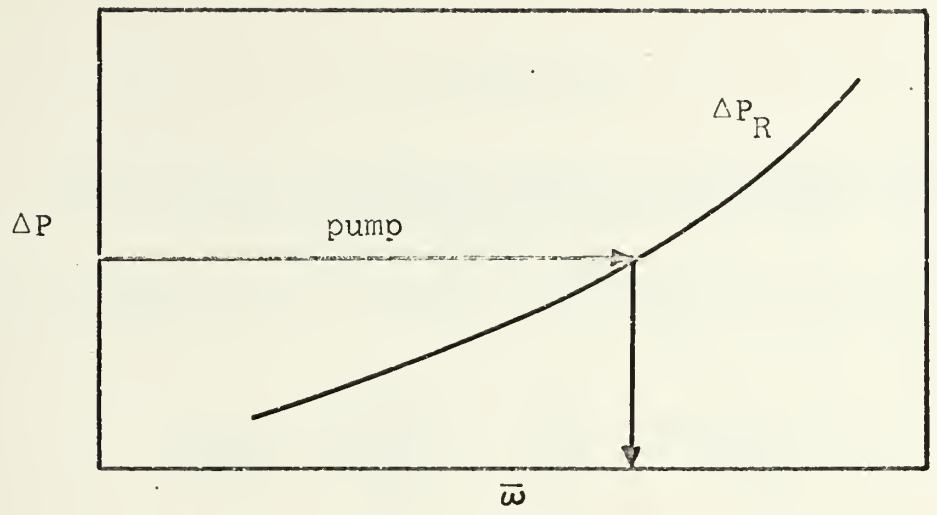

a. Relationship between driving pressure and mass flow rate in a forced convection system where, for a fixed Δt, $\bar{q}' = \bar{\omega} c_p \Delta t / n_r l$, and $\bar{\omega}$ depends on the pump pressure.

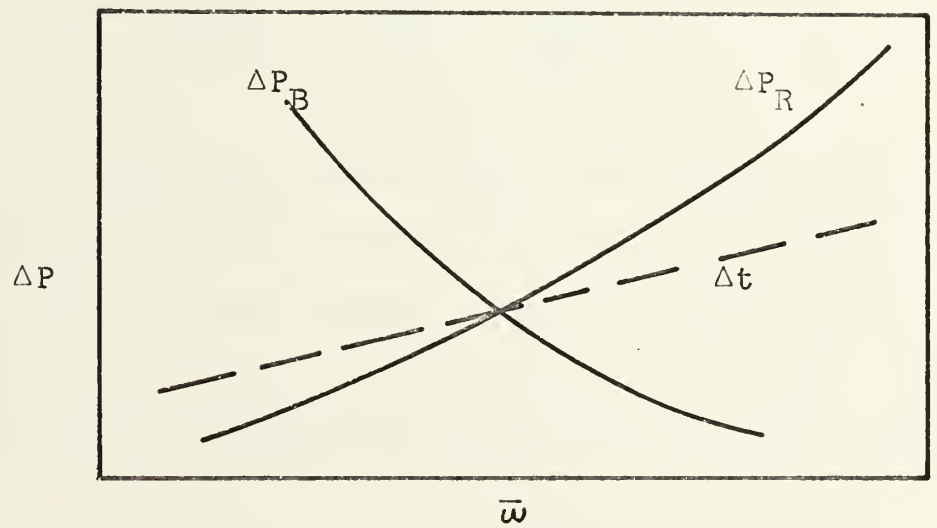

b. Relationships between driving pressure, mass flow rate, and core temperature rise in a natural convection system where, for a fixed Δt, $\bar{q}' = \bar{\omega} c_p \Delta t / n_r l$ is found by Eq. (A-10), and $\bar{\omega}$ is determined as the intersections of lines of Δt, ΔP_B, and ΔP_R.

Fig. A.3. Comparison of driving forces in forced and natural convection.

Appendix B

Derivation of Hydraulic Diameters as Functions of Pitch and Diameters of Fuel Pins

Refer to Fig 1.1 for finding fuel volume fractions, V_f':

$$(V_f')_h = \frac{2\pi d_p^2/4}{6\frac{1}{2}p\frac{p}{2}\sqrt{3}} = \frac{\pi d_p^2}{3\sqrt{3}p_h^2} = \frac{\pi\sqrt{3}}{9}\left(\frac{d_p}{p_h}\right)^2 , \qquad \text{(B-1)}$$

$$(V_f')_t = \frac{\frac{\pi}{2}d_p^2/4}{\frac{1}{2}p\frac{p}{2}\sqrt{3}} = \frac{\pi d_p^2}{2\sqrt{3}p_t^2} = \frac{\pi\sqrt{3}}{6}\left(\frac{d_p}{p_t}\right)^2 , \qquad \text{(B-2)}$$

$$(V_f')_{sq} = \frac{\pi d_p^2/4}{p^2} = \frac{\pi}{4}\left(\frac{d_p}{p_{sq}}\right)^2 . \qquad \text{(B-3)}$$

In the derivations of the linear power output capabilities of the lattices, the assumptions made were that the same fuel pin diameter was to be used in each lattice, and the fuel volume fractions were to be equal. Hence, we obtain the following relations between lattice pitches:

$$(V_f')_h = (V_f')_t ,$$

$$\frac{\pi}{3\sqrt{3}}\left(\frac{d_p}{p_h}\right)^2 = \frac{\pi}{2\sqrt{3}}\left(\frac{d_p}{p_t}\right)^2 ,$$

and

$$p_t^2/p_h^2 = 3/2 . \qquad \text{(B-4)}$$

In like manner

$$p_{sq}^2/p_h^2 = 3\sqrt{3}/4 \qquad \text{(B-5)}$$

By definition $D_e = \dfrac{4 \times \text{cross sectional flow area}}{\text{wetted perimeter}}$:

$$(D_e)_h = \frac{4(\frac{1}{2}6p_h(p_h/2)\sqrt{3} - 2\pi d_p^2/4)}{2\pi d_p} = \frac{3\sqrt{3}p_h^2 - \pi d_p^2}{\pi d_p}, \qquad \text{(B-6)}$$

$$(D_e)_t = \frac{4(\frac{1}{2}p_t(p_t/2)\sqrt{3} - \frac{1}{2}\pi d_p^2/4)}{\frac{1}{2}\pi d_p} = \frac{2\sqrt{3}p_t^2 - \pi d_p^2}{\pi d_p}. \qquad \text{(B-7)}$$

Using Eq. (B-4),

$$(D_e)_t = \frac{2\sqrt{3}(\frac{3}{2}p_h^2) - \pi d_p^2}{\pi d_p} = (D_e)_h, \qquad \text{(B-8)}$$

$$(D_e)_{sq} = \frac{4(p_{sq}^2 - \pi d_p^2/4)}{\pi d_p} = \frac{4p_{sq}^2 - \pi d_p^2}{\pi d_p}. \qquad \text{(B-9)}$$

Using Eq. (B-5),

$$(D_e)_{sq} = \frac{4(\frac{3\sqrt{3}}{4}p_h^2) - \pi d_p^2}{\pi d_p} = (D_e)_h. \qquad \text{(B-10)}$$

The above results show that for equal pin diameters and fuel volume fractions, the equivalent diameters of the three lattices are equal.

Appendix C

Lattice Parameters

Table C.1 lists some of the lattice parameters which are being used in current large LMFBR's and which are proposed for future large LMFBR's. Table C.2 and Fig. C.1 show volume fraction of fuel and triangular lattice pin pitch and gap spacing based on a gap spacing of 0.040 inches for the open-hexagonal lattice (the minimum assumed practical) and equal pin diameters for both lattices.

The equations used in these calculations are Eq. (B-1) and Eq. (B-2). The calculation procedure was to select d_p and, using $\delta_h = 0.040$ inches, compute p_h and $(V_f')_h$ from Eq. (B-1). Then taking $(V_f')_h = (V_f')_t$, p_t and δ_t are computed from Eq. (B-2) for the same assumed pin diameter. Fig. C.1 shows that as d_p decreases, δ_t approaches δ_h with an accompanying drop in V_f'. For reasonable pin sizes as shown, and constraints of constant d_p and V_f' between lattices, the following conclusions are drawn:

1. The pin to pin gap for a triangular lattice (0.120 in.) is considerably larger than that for an open-hexagonal lattice (0.040 in.).
2. The fuel volume fraction for the lattices with reasonable pin diameters (0.250 to 0.300 inches) are about 0.45 to 0.47. Significant increases above these values require large (and uneconomical) increases in pin diameter.

Table C.1

Current and Proposed LMFBR Parameters

	A. I.[15A]	B. W.[15B]	C. E.[15C]	G. E.[15D]	W.[15E]
SYSTEM PARAMETERS					
Electrical power (MWe)	1004	1008	1000	----	1055
Thermal efficiency	40.7	41.2	40.6	----	40.6
Thermal power (MWt)	2500	2450	2465	2417	2600
Inlet temperature (^{o}F)	760	800	797	810	770
Outlet temperature (^{o}F)	1060	1100	1095	1150	1000
System pressure (psig)	35	----	----	----	----
secondary	2400	2400	2400	----	2446
Flow rate (lb./hr. x 10^{6})	93.0	83.8	94.0	----	127.4
CORE AND BLANKET DIMENSIONS					
Core: height (in.)	50.0	34.7	24.0	30.0	40.0
diameter (in.)	92.5	120.0	107.0	97.4	92.5
Blanket: thickness (in.)	----	----	axial 18.0 radial 6.0	15.0	10.5
Control rods	15	----	22	31	57
NUCLEAR PARAMETERS					
Fuel: enrichment (%)	inner 11.6 outer 16.0	11.6	10.13 12.05	10.73 13.45	15.0 18.0

Table C.1. continued

	A. I.	B. W.	C. E.	G. E.	W
Core comp. (vol. %) fuel	31.0 (UO_2)	44.2 (UO_2)	38.6 (UC)	46.7 (UO_2)	29.2
sodium/steel	50.1/18.9	35.3/16.9	40.0/13.1	38.0/14.9	52.2/12.5
Critical mass Pu (kg)	2187	2770	----	1624 fissile	----
Breeding ratio core/blanket	0.83/0.49	0.93/0.43	1.50	1.40	1.32
Doubling time (yr)	10.0	10.4	7.0	7.75	11.0
Sodium void reactivity ($)	6.82	7.50	3.20	----	10.4
ASSEMBLY PARAMETERS					
Number of pins in core	56,500	----	35,700	----	40,300
Pin diameter/pitch (in/in)	0.250/0.310	0.280/----	0.400/0.451	0.250/0.300	0.302/0.375
Fuel length (in)	50.0	----	24.0	30.0	40.0
Gas plenum length (in)	64.0	----	----	----	----
Axial blanket length (in)	24	----	18	----	15
Pin support method	grid	----	wire wrap	undecided	undecided
PERFORMANCE PARAMETERS					
Ave. linear power (kWt/ft)	10.0	10.2	29.5	----	18.7
Ave. power density (kWt/l)	500	----	----	----	----
Ave. spec. power (kWt/kg)	168	885	121.5	1,304	168.2

Table C.1. continued

	JAERI[15F]	FFTF[14]	PHENIX[17]	PFR[18]
SYSTEM PARAMETERS				
Electrical power (MWe)	----	----	250	----
Thermal efficiency	40.0	----	----	----
Thermal power (MWt)	2,500	400	563	----
Inlet temperature (^{o}F)	752	600	752	----
Outlet temperature (^{o}F)	1,166	900	1,040	1040 - 1110
System pressure (psig) primary	----	35	----	----
secondary	3,500	----	----	----
Flow rate (lb/hr x 10^{6})	88.4	----	21.9	----
CORE AND BLANKET DIMENSIONS				
Core: height (in)	31.5	----	33.4	----
diameter (in)	104	----	53.4	----
Blanket thickness (in)	15.7	----	axial 11.8 radial 9.85	----
Control rods	12	----	6	----
NUCLEAR PARAMETERS				
Fuel: enrichment (%)	inner 9.5 outer 13.0	----	20.3 27.4	----

Table C.1. continued

	JAERI	FFTF	Phenix	PFR
Core comp. (vol. %) fuel	44.2 (UO_2)	----	36.8 (UO_2)	UO_2
sodium/steel	39.0/16.0	----	29.7/----	----
Critical mass Pu (kg)	total 2,350 fissile 1930	----	700	----
Breeding ratio, core/blanket	0.96/0.48	----	0.54/0.62	----
Doubling time (yr)	7.2	----	17.0	----
Sodium void reactivity ($)	3.1	----	----	----
ASSEMBLY PARAMETERS				
Number of pins in core	89,300	16,275	11,900	----
Pin diameter/pitch (in/in)	0.250/0.304	0.235/0.291	0.260/----	0.230/----
Fuel length (in)	31.5	36.0	----	36.0
Gas plenum length (in)	23.6	41.0	16.5	----
Axial blanket length (in)	15.75 x 2	12.0	----	18.0
Pin support method	wrapper tube	----	spiral wire	grid
PERFORMANCE PARAMETERS				
Ave. linear power (kWt/ft)	9.5	7.0	13.1	13.7 peak
Ave. power density (kWt/l)	500	386	422	371
Ave. specific power (kWt/kg)	1140	146	----	250 peak

Table C.2

Pin to pin spacing and pin pitch for triangular and open-hexagonal lattices which have equal pin diameters and equal volume fractions of fuel.

d_p (in.)	δ_h (in.)	V_f'	δ_t (in.)	p_h (in.)	p_t (in.)
0.25	0.040	0.450	0.105	0.290	0.355
0.30	0.040	0.472	0.116	0.340	0.416
0.35	0.040	0.488	0.127	0.390	0.477
0.40	0.040	0.501	0.138	0.440	0.538
0.45	0.040	0.512	0.156	0.490	0.606
0.50	0.040	0.519	0.160	0.540	0.660

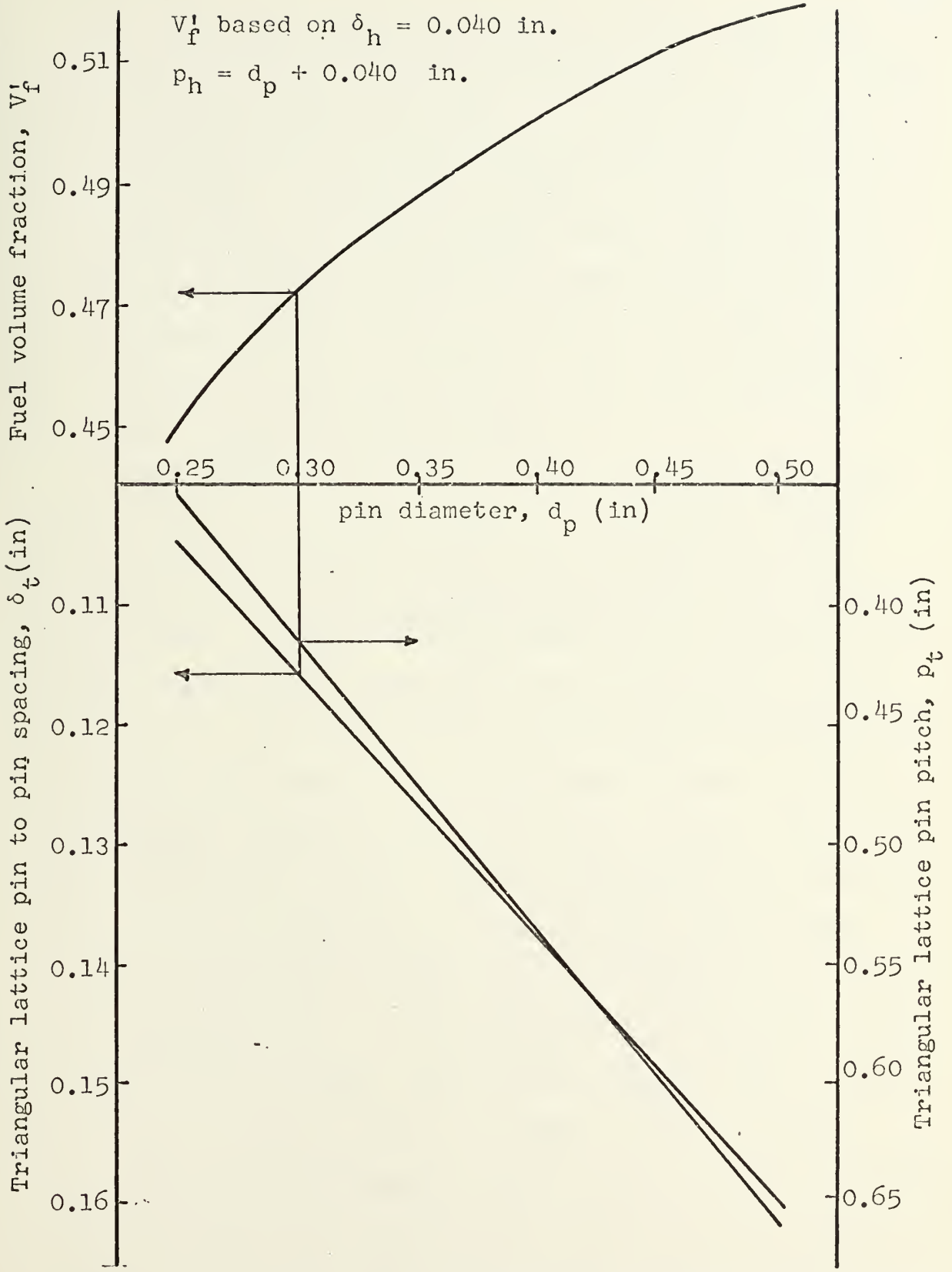

Fig. C.1. Assumed and calculated parameters for the open-hexagonal and triangular lattices.

3. The fuel volume fraction, V_f', used in the above calculations was based on a single fuel cell in a fuel subassembly and was equal to 1 - V_{Na}(sodium volume fraction). Taking into account the volume of the core taken up by the clad, the gap between clad and fuel, the subassembly housing, the space between subassemblies, and the control assemblies, the actual fuel volume fraction, V_f, for the whole core is 0.306, as will be shown in detail below.

Refer to Fig. C.2 for calculation of the actual core fuel volume fraction, V_f. The fuel subassembly contains 217 fuel pins of 0.300 inches outside diameter and has a V_f' of 0.472. Based on a unit length of fuel assembly, the inside volume of the fuel subassembly is $217V_{\text{fuel pin}}/V_f' = 32.2$ in.^{3}. Dividing the subassembly into six equilateral triangles, the height, h, of a triangle becomes one half the internal distance across the flats. Using a wall thickness of 0.150 in. and one half the subassembly to subassembly spacing of 0.025 in., the subassembly pitch divided by two is $h' = h + 0.175$ in. One equilateral triangle of the subassembly has a volume of $\frac{1}{6}(32.2) = 5.37$ in.^{3}. The volume of one triangle equals $\frac{1}{2}bh = \frac{1}{2}(\frac{2h}{\sqrt{3}})h = \frac{\sqrt{3}}{3}h^2 = 5.37$ in.^{3} or $h = 3.04$ in. Now $h' = 3.04 + 0.175 = 3.215$ in. The volume each subassembly occupies, V_{SA}, in the core based on the distance from subassembly center across the flats to the midpoint between subassemblies is $V_{SA} = 6(\frac{1}{2}b'h')$

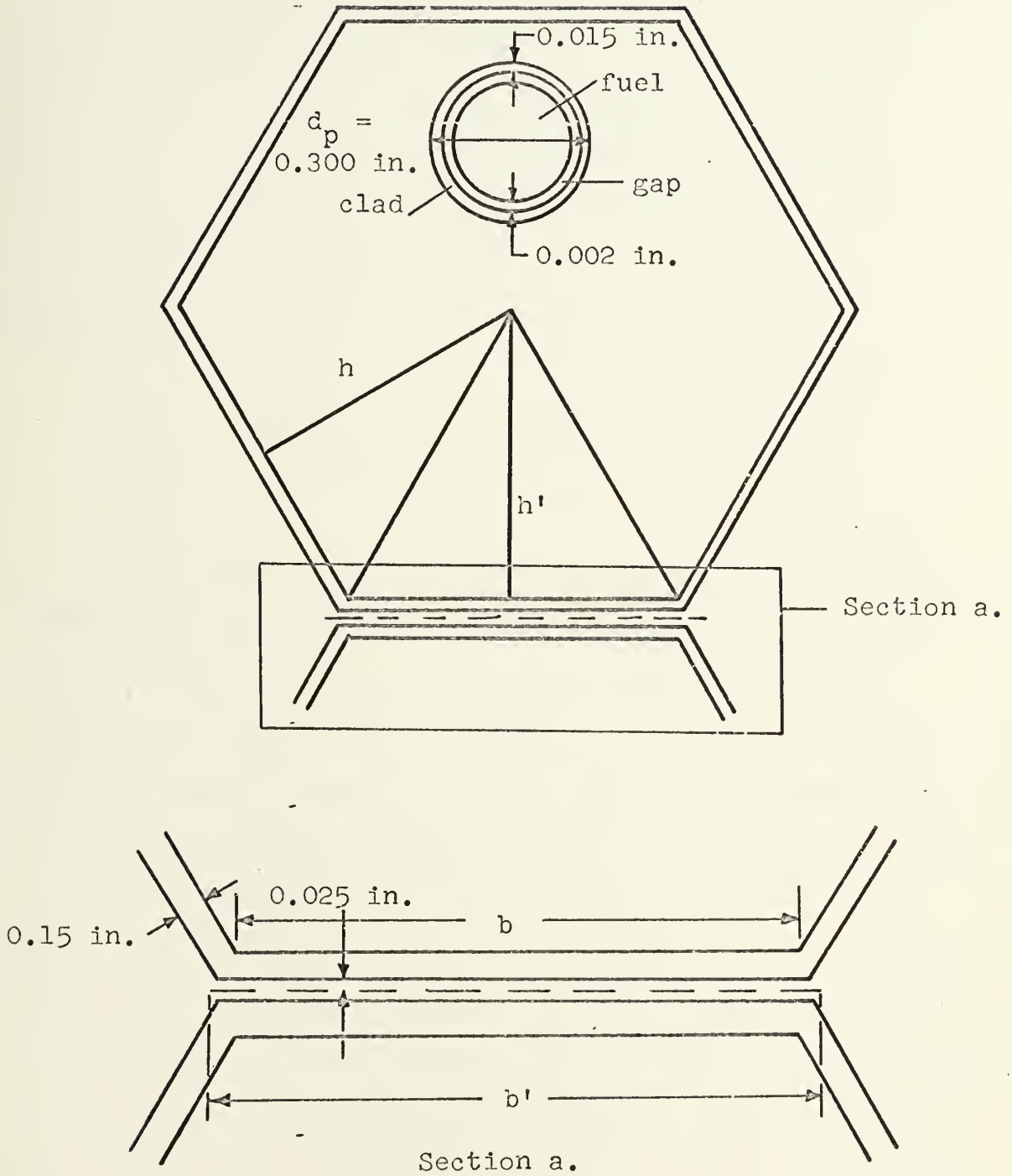

Fig. C.2. Core subassembly configuration

$= 6(\frac{1}{2}(\frac{2\sqrt{3}}{3}h')h') = 2\sqrt{3}h'^2 = 35.75$ in.^{3}. Using a pin diameter of 0.300 in., a clad thickness of 0.015 in., and a fuel to clad radial gap of 0.002 in., the volume of fuel in a subassembly is $V_{fuel} = (217)\frac{\pi(0.300 - 0.034)}{4} = 12.06$ in.^{3}. Assuming there is one control assembly for every ten fuel subassemblies, the actual fuel volume fraction in the core, V_f, is

$$V_f = \frac{V_{fuel}}{V_{SA} + \frac{1}{10}V_{SA}} = \left(\frac{12.06}{35.75 + 3.575}\right) = 0.306$$

This number is low compared to the fuel volume fractions (V_f = 29.2 to 46.7) of the reactors in Table C.1. Our value of V_f does not take into consideration the irradiation induced swelling of the stainless steel subassembly walls. Because of this swelling the subassembly to subassembly spacing must be 0.25 inches instead of 0.05 inches. Therefore, $h' = 3.04 + 0.275 = 3.315$ in., and $V_{SA} = 38.07$ in.^{3}. Consequently, our value of V_f is lower: $V_f = 0.288$. The fuel volume fractions of the cores in Table C.1 do not reflect the stainless steel swelling. The methods used to calculate the volumetric compositions of the cores for the reactors in Table C.1 were not explained in the references cited. Therefore, it is difficult to make a good comparison of the volumetric compositions of the actual cores in Table C.1 and our theoretical core. However,

if the V_f of 0.306 is too low for practical use, an increased pin diameter is feasible with the use of uranium carbide fuel which has a higher melting point than does uranium dioxide fuel. Some designs are proposing pin diameters of 0.400 inches for future 1000 Mwe LMFBR's fueled with UC[15c].

Appendix D

Relative Linear Power Output for Various Lattice Configurations Under Forced Circulation

The average linear power output of a lattice flow cell is given by

$$\overline{q}' = \frac{\overline{\omega} c_p \Delta t}{n_r l} , \qquad \text{(D-1)}$$

where

$$\overline{\omega} = \rho A \overline{V}$$

Assuming the pumps are moving the coolant at the same total rate through the three lattices, and in view of the fact that the volumetric compositions of the three lattices are equal, the coolant velocity will be the same in the three lattices. It is shown in Appendix B that the equivalent diameters of the three lattices are equal. The lattices have the following numbers of effective rods per flow cell: $(n_r)_h = 2$; $(n_r)_t = 1/2$; $(n_r)_{sq} = 1$.

Since

$$A = \frac{D_e \times (\text{wetted perimeter})}{4} , \qquad \text{(D-3)}$$

$$A_h = \frac{D_e(2\pi d_p)}{4} = \frac{D_e \pi d_p}{2} , \qquad \text{(D-4)}$$

$$A_t = \frac{D_e(\frac{1}{2}\pi d_p)}{4} = \frac{D_e \pi d_p}{8} = \frac{1}{\pi} A_h , \qquad \text{(D-5)}$$

$$A_{sq} = \frac{D_e(\pi d_p)}{4} = \frac{1}{2}A_h \quad . \qquad \text{(D-6)}$$

Using the above expressions for flow areas in Eq. (D-2), which is substituted into Eq. (D-1), gives the following relative values for the linear power output of the three lattices:

$$\frac{\overline{q}'_h}{\overline{q}'_t} = \frac{\rho A_h V c_p \Delta t/2l}{\rho A_t V c_p \Delta t/\frac{1}{2}l} = \frac{A_h/2}{\frac{1}{4}A_h/\frac{1}{2}} = 1$$

$$\frac{\overline{q}'_h}{\overline{q}'_{sq}} = \frac{\rho A_h V c_p \Delta t/2l}{\rho A_{sq} V c_p \Delta t/l} = \frac{A_h/2}{A_h/2} = 1$$

$$\frac{\overline{q}'_t}{\overline{q}'_{sq}} = 1$$

The above ratios show that the linear power output for the three lattices are equal under forced circulation for equal V'_f and d_p.

The pressure losses through the different lattices are the same since

$$\Delta P = f_F \frac{4l\rho V^2}{D_e 2g_c} \quad , \qquad \text{(D-7)}$$

and all the parameters in Eq. (D-7), including f_F and D_e, are equal for the three lattices. The corresponding coolant

velocities, V, are shown to be equal in the lattices in Tables IV.1 and IV.3. The forced convection heat transfer coefficients are also the same for the three lattices since

$$Nu = hD_e/k = C_1 + C_2(Pe)^n,$$

$$Nu = C_1 + C_2(D_e V\rho c_p/k)^n, \qquad \text{(D-8)}$$

and all the values in Eq. (D-8) are again equal for the three lattices, including the D_e's as discussed in Appendix B.

From the above ratios and correlations it is seen that the linear power output, pressure drop, and heat transfer characteristics are the same for the three lattice configurations.

Appendix E

References

1. E. B. Ash, "Heat Transfer in Fast Breeder Nuclear Reactors", paper presented at the Education and Creative Engineering Synposium, M.I.T., April, 1969.

2. H. H. Hummel and D. Okrent, Reactivity Coefficients in Large Fast Power Reactors, American Nuclear Society, 1970.

3. C. W. Monroe, Sodium Void Coefficient of Reactivity, a Review and Study of Analytical Work, UNC-2190, United Nuclear Corp., White Plains, New York, May 1965.

4. T. Lacapelle, internal CEA report, June, 1964.

5. P. Benoist, "Théorie du coefficient de diffusion dans un réseau comportant des cavites", CEA report No. 2278, January, 1964.

6. D. J. Behrens, "The Effect of Holes in a Reacting Material on the Passage of Neutrons", Proceeding of the Physical Society of London, 62A: 607, 1949.

7. L. S. Tong, "Pressure Drop Performance of a Rod Bundle", presented at the Winter Annual Meeting of the ASME, New York, New York, December, 1968, Rod Bundle Symposium.

8. A. N. de Stordeur, "Drag Coefficients for Fuel Element Spacers", Nucleonics, Vol. 19, No. 6, June, 1961.

9. W. M. Kays and A. L. London, Compact Heat Exchangers, National Press, Inc., Palo Alto, California, 1955.

10. W. M. Kays, Convective Heat and Mass Transfer, McGraw Hill Book Co., Inc., New York, 1966.

11. R. G. Deissler and M. F. Taylor, TID-7529, Reactor Heat Transfer Conference, New York, pt. 1, book 1, November, 1957.

12. H. Schlichting, Boundary Layer Theory, McGraw Hill Book Co., Inc., New York, 1955.

13. D. J. Bender and P. M. Magee, Turbulent Heat Transfer in a Rod Bundle With Liquid Metal Coolant, GEAP-10052, AEC Research and Development Report, July, 1969.

14. N. E. Todreas, MIT, private communication.

15A* Atomics International, 1000-MWe LMFBR Follow-on Study, November, 1968.

15B* Babcock and Wilcox, 1000-MWe LMFBR Follow-on Study, November, 1968.

15C* Combustion Engineering, Inc., 1000-MWe LMFBR Follow-on Study, November, 1968.

15D* General Electric Co., 1000-MWe LMFBR Follow-on Study, November, 1968.

15E* Westinghouse Electric Corp., 1000-MWe LMFBR Follow-on Study, November, 1968.

15F* Japan Atomic Energy Research Institute, JAERI Presentation, November, 1968.

16. C. F. Bonilla, "Heat Removal", Nuclear Engineering, C. F. Bonilla, ed., McGraw Hill Book Co., Inc., New York, 1957.

17. USAEC, TID-4500, Phenix, Prototype Fast-Neutron Nuclear Power Station, AEC-tr-7130, February, 1970.

18. P. V. Evans, ed., Fast Breeder Reactors, Proceedings of the London Conference on Fast Breeder Reactors, British Nuclear Energy Society, May, 1966, Pergamon Press, New York, 1967.

---

* References (15A) through (15F) were presented at the International Conference on Sodium Technology and Large Fast Reactor Design, Argonne National Laboratory, ANL-7520, November, 1968.

Appendix F

Nomenclature
(unless defined as they appear)

English	Meaning	Units
A	cross sectional flow area	ft^2, $in.^2$
c_p	heat capacity	BTU/lb-^oF
d,D	diameter	ft, in.
f	friction factor	----
g_c	gravitational constant	ft/hr^2
h	heat transfer coefficient	BTU/hr-ft^2-^oF
k	thermal conductivity	BTU/hr-ft-^oF
k	multiplication factor	----
l	length	ft, in.
n	a quantity	----
N	pipe length	ft
Nu	Nusselt number	----
$\bar{q}$	average power output per cell	kw
$\bar{q}'$	average linear power output per pin	kw/ft
p	pitch	in.
P	perimeter	in.
Pe	Peclet number	----
ΔP	pressure drop	lb/ft^2, psi
r	radius	in.
Re	Reynolds number	----
S	cross sectional flow area	ft^2, $in.^2$

English	Meaning	Units
Δt	axial temperature difference per cell (inlet to outlet)	^{o}F
$\overline{V}$	average coolant velocity	ft/hr
V_f'	fuel volume fraction = 1 - V_{Na} where V_{Na} is the sodium volume fraction	----
V_f	Actual fuel volume fraction in a real core	----
z	height	ft
Z	elevation difference	ft

Greek

β	fraction of delayed neutrons	----
β	temperature coefficient of volumetric expansion	$^{o}F^{-1}$
δ	pin to pin spacing	in.
δ	boundary layer thickness	in.
μ	dynamic viscosity	lb/ft-hr
ν	kinematic viscosity	ft^2/hr
ρ	density	lb/ft^3
σ	ratio of areas, A_2/A_1	----
$\overline{\omega}$	average mass flow rate per flow cell	lb/hr

Subscripts

B	due to buoyancy forces
e	equivalent
em	empirical
E	entrance, exit

Subscripts	Meaning
g	grids
h	open-hexagonal lattice
hy	hydraulic
p	pin
r	rods
R	due to friction
s	spacers
SA	subassembly
sq	square
t	triangular lattice
th	theoretical
T	total
W	wetted
1	away from gridded region
2	in gridded region